IJCIET

INTERNATIONAL JOURNAL OF CIVIL ENGINEERING AND TECHNOLOGY

Journal ID: 6971-8185

IAEME Publication

Chennai, India

editor@iaeme.com/ iaemedu@gmail.com

https://iaeme.com/Home/journal/IJCIET

International Journal of Civil Engineering and Technology (IJCIET)
Volume 17, Issue 2, March-April 2026, pp. 13-57, Article ID: IJCIET_17_02_002
Available online at https://iaeme.com/Home/issue/IJCIET?Volume=17&Issue=2
ISSN Print: 0976-6308; ISSN Online: 0976-6316
Impact Factor (2026): 27.65 (Based on Google Scholar Citation)
Journal ID: 6971-8185; DOI: https://doi.org/10.34218/IJCIET_17_02_002

INTEGRATED SEISMIC-HYDRAULIC PERFORMANCE ASSESSMENT OF A ZONED EMBANKMENT DAM: APPLICATION TO THE MEMVE'ELE HYDROPOWER PROJECT (CAMEROON)

Gérard Ghislain SENGHA[1]

Department of Physics, Faculty of Sciences, University of Bangui, P.O. Box 1450, Bangui, Central African Republic.

Paul NDY VON KLUGE[2,†]

Laboratory of Mechanics, Department of Physics, Faculty of Sciences, University of Yaounde I, P.O. Box 812, Yaoundé, Cameroon.

University Institute of Wood Technology, Civil Engineering, University of Yaounde I, P.O. Box 306, Mbalmayo, Cameroon.

Bénoît DOUMIA[3]

Laboratory of Mechanics, Department of Physics, Faculty of Sciences, University of Yaounde I, P.O. Box 812, Yaoundé, Cameroon.

High School of Technology, University of Bangui, Central African Republic.

†Corresponding Author: Paul NDY VON KLUGE

ABSTRACT

This study examines the coupled seismic-hydraulic response of the Memve'ele zoned embankment dam in Cameroon under multi-component seismic excitation. Conventional dam safety assessments often consider only translational ground motions and two-dimensional analyses, which may underestimate the influence of rotational and torsional seismic components on the response of large embankment dams. To address

this limitation, an integrated numerical framework is developed that combines finite-element seepage, stability, and stress-strain analyses in GeoStudio with external computational routines implemented in MATLAB. The methodology enables pseudo-three-dimensional seismic loading by incorporating translational, rocking, and torsional motion components into multiple two-dimensional model slices. Seepage and transient hydraulic analyses are conducted to evaluate phreatic surface evolution, pore-water pressure distribution, and slope stability during reservoir operation. Dynamic response analysis is then performed to assess deformation patterns, stress redistribution, and safety factors under coupled hydraulic-seismic loading. Results indicate that the permeability and mechanical properties of the clay core strongly influence downstream seepage and stability conditions, while rotational seismic components significantly modify stress concentrations and displacement patterns within the dam body. The proposed semi-three-dimensional approach provides a practical tool for improving seismic safety assessment of zoned embankment dams.

Keywords: Embankment dam, rotational ground motion, torsional excitation, seismic response, seepage analysis, GeoStudio

Cite this Article: Gérard Ghislain SENGHA, Paul NDY VON KLUGE, Bénoît DOUMIA. (2026). Integrated Seismic-Hydraulic Performance Assessment of a Zoned Embankment Dam: Application to the Memve'ele Hydropower Project (Cameroon). *International Journal of Civil Engineering and Technology (IJCIET)*, 17(2), 13-57.
DOI: https://doi.org/10.34218/IJCIET_17_02_002

1. INTRODUCTION

Modern dams are broadly classified into two main categories: embankment dams and concrete dams. Embankment dams represent approximately 85% of existing structures worldwide and are further divided into earth-fill and rock-fill dams. The choice of dam type depends on topographic, geological, hydrological, and socio-economic factors, with an overarching goal of ensuring safety against overtopping and internal erosion. Earth dams, in particular, are constructed using locally available materials to maintain structural stability and water tightness under operational and extreme loading conditions [8, 17].

In the African context, large embankment dams such as Kariba (Zambia-Zimbabwe), Akosombo (Ghana), and Memve'ele (Cameroon) play a central role in energy security and regional development. However, many of these projects are located in tectonically active

regions or near zones of moderate seismicity, raising concerns over their long-term safety under coupled seismic-hydraulic loading. This makes seismic performance assessment a critical component of dam engineering in Africa.

Traditionally, seepage and slope stability analyses have been conducted using Darcy's law (1856) to model flow through porous media, supplemented by classical stability methods such as the Ordinary Method of Slices (Fellenius, 1936) [35] and later by finite element formulations (Zienkiewicz and Chung, 1967) [20]. Over the past decades, numerical tools such as ANSYS and Geo-Studio have been widely applied to assess seepage, slope stability, and failure mechanisms in earth dams [32, 19]. More recent studies have examined horizontal drain efficiency, mesh sensitivity, and advanced coupled flow-deformation formulations for dam safety evaluation [1, 34, 29, 15].

Parallel to hydraulic considerations, the dynamic response of dams under seismic loading has been extensively studied, especially following landmark earthquakes such as 1964 Niigata, 1999 Chi-Chi, and 2008 Wenchuan. Research has highlighted the importance of non-linear soil behavior, dam-foundation interaction, and hydrodynamic pressures on dam performance [22, 16, 5, 31]. Nevertheless, most design codes and practical assessments continue to rely primarily on translational ground motion inputs. Recent advances in seismology and engineering mechanics emphasize the role of rotational and torsional ground motion components [23, 33, 7, 3, 28]. These components, variously defined as free-field, chord, or point rotations, remain underexplored in dam engineering despite their potential to alter stress distributions, seismic demand, and soil-structure interaction effects [6, 4]. The absence of consensus in the literature underscores a research gap: the limited incorporation of rotational and torsional excitations into dam safety analyses, particularly for large embankments in developing regions.

Another limitation is the prevalent reliance on two-dimensional (2D) modeling approaches, which although computationally efficient cannot fully capture the complexity of three-dimensional (3D) ground motion fields and structural responses. This shortcoming is especially critical for zoned embankment dams, where material heterogeneity, abutment interaction [11], and differential stiffness effects introduce strong three-dimensionality.

Research Objective

In response to these challenges, the present study develops an integrated methodology for the coupled seismic-hydraulic analysis of embankment dams, with a focus on the Memve'ele hydroelectric dam in Cameroon. The approach combines:

- finite element simulations in Geo-Studio to model seepage, stability, and soil-structure interaction,
- and external coupling with MATLAB routines to perform seismic motion decomposition (translational, rotational, and torsional components) and to apply these as boundary inputs in multiple 2D slices.

This integrated framework enables the assessment of pore water pressure evolution, slope stability, and dynamic resilience under realistic multi-component ground motions. The contributions are twofold: (i) providing new insights into coupled seismic-hydraulic dam safety in Africa, and (ii) addressing methodological gaps in the treatment of rotational and torsional ground motions within finite element dam analyses.

This study contributes to the seismic safety assessment of large embankment dams by introducing a pseudo-three-dimensional framework that integrates translational, rocking, and torsional ground-motion components into a coupled hydraulic-dynamic numerical analysis. The methodology is applied to the Memve'ele hydropower dam, providing insight into the influence of rotational seismic components on stress redistribution and slope stability.

The remainder of this paper is structured as follows: Section 2 introduces the methodology and numerical framework. Section 3 presents the geological setting and seismicity of southern Cameroon. Section 4 discusses the numerical results and implications for dam safety. Section 5 concludes the study.

2. MATERIALS AND METHODS

The Memve'ele embankment dam is an earth-fill structure with a total height of 25 m, a crest length of approximately 1850 m (with a zoned section of 625m), and a crest width of 10 m, see right side Fig. 2. The spillway bridge is composed of simply supported precast bridge girders, Fig. 3(b), therefore the transverse (in cross-river direction) deformations of the pier are not restrained by the spillway bridge. The portal crane beam of the spillway and flushing sluice is located upstream of the spillway and flushing sluice. The length of the portal crane

beam is 12.65m (each span), and the section is 'T' type. There is a rail fixed on the top of the crane beam, Fig. 2. Crane wheels can roll on the rail.

This section describes the geometric configuration, material properties, and hydraulic and seismic modeling approaches.

The numerical framework developed to assess the coupled seismic– hydraulic performance of the Memve'ele embankment dam. The methodology integrates finite element analyses performed in Geo-Studio with external routines in MATLAB to approximate the effects of three-dimensional ground motion components on a zoned earth dam.

2.1 Dam Geometry and Material Zoning

The upstream slope is designed at 1V:3H, while the downstream slope is 1V:2.5H. A central clay core ensures impermeability, flanked by transition filters and rock-fill shells for stability and drainage. Figure 1 presents the zoned geometry, and Table 1 summarizes the material zoning.

Table 1: Zoning configuration of the Memve'ele dam.

Zone	Material	Function
Core	Low-plasticity clay	Impermeable barrier
Filters	Sand-gravel	Transition and drainage
Shell (upstream)	Rock-fill	Stability and wave protection
Shell (downstream)	Rock-fill	Stability and drainage
Foundation	Residual soil over granite	Load-bearing support

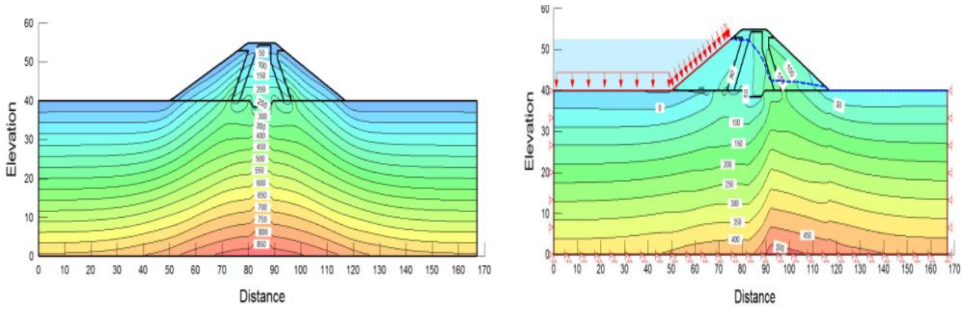

(a) (b)

Figure 1: Contour plots showing maximum stress and mean stress distribution in the dam body.

Figure 1 presents maximum and mean stress of Dam (kPa) respectively. These figures combined seismic-hydraulic response, coupled pore pressure and deformation trends and critical zones of instability. Plot equipotential lines and flow paths, Figure 1, and the figures down verify effectiveness of clay core in keeping downstream slope dry, displacement fields (translational vs. rotational vs. torsional excitation and stress distribution in core and shells.

2.2 Soil Parameters and Input Data

Representative soil parameters were derived from site investigations and laboratory tests. The key geotechnical properties are summarized in Table 2. Parameter selection follows regional studies [22, 5, 33] and comparable embankment dam projects in West Africa.

Table 2: Soil and material properties used in the numerical simulations.

Material	γ (kN/m^3)	c (kPa)	φ (°)	k (m/s)
Clay core	18.5	25	24	1.0×10^{-9}
Filter (sand-gravel)	20.0	0	36	1.0×10^{-3}
Rock-fill shell	21.0	0	42	5.0×10^{-2}
Residual soil (foundation)	19.0	10	28	1.0×10^{-5}
Weathered granite (foundation)	22.0	15	35	1.0×10^{-6}

Upon the Right side of the main spillway, the wing walls are arranged along the upstream and downstream dam slope of earth dam for earth retention. The upstream wing wall has a length of 62.958m in downstream flow. After the top elevation of the wing wall is lowered from 395.0m to 385.0m along the dam slope, then the flat top comes into being. The upstream wing wall at 8m from the front edge of overflow weir takes turns at an arc with a radius of 35m from the end of the apron should parallels with the dam axis instead of running along the downstream flow.

Both upstream and downstream wing walls adopt the semi-gravity concrete retaining wall. The wall is erected facing the water surface while the plane is set in the form of a straight line and circular arc. The upstream wing wall is 44.8m long along the water flow. Figure 2 provides frame structure mechanics model, ie. the key plan of main spillway and flushing sluice. The right side shows the body of the dam.

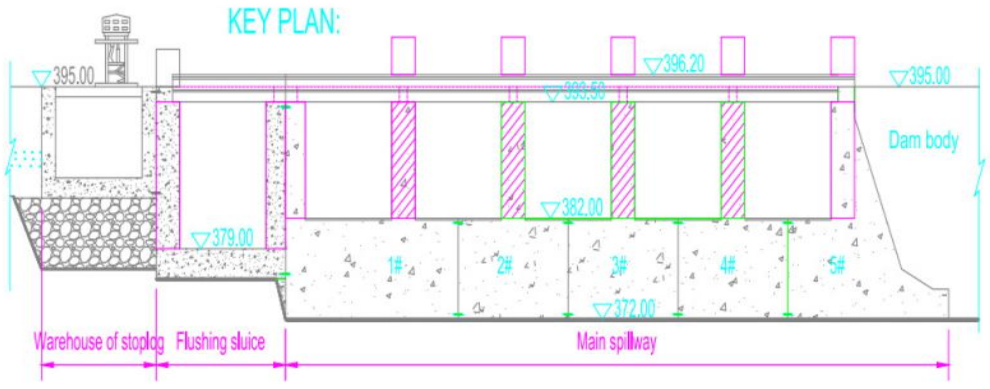

Figure 2: Structural frame model of the spillway and flushing sluice showing the key layout of the dam and adjacent structures.

2.3 General formulation

To provide key dynamic parameters influencing the seismic response of multi-component systems, the collision is highlighted, see Fig. 3 [9, 14], and the pounding forces are suggested in the equation of motion comprehensively than using nonlinear viscoelastic model [9]. Fig. 3(b) shows the model of simply supported precast bridge girders that could be affected during seismic response.

2.4 Engineering Situation

Both the left and right sides of the control section of the main spillway are separately connected to the flushing sluice and earth dam. The main spillway of the Memve'ele hydroelectric project is located on the left side of the main dam, adjacent to the power intake. There are five openings for flood discharge and one opening for sand flushing Fig.4. The crest elevation and total length of the main spillway are 382m and 85m respectively. Fig.4(a) represents the girder vibration up to the main spillway and flushing sluice with on-site elevations. Fig.4(b) gives the desk sequence and expansion joints layout.

The flushing sluice and main spillway are located on the main channel on the left bank of the main dam. The upstream on the left side of the main spillway and flushing sluice is connected to the connecting dam on the left bank; both left and right sides of the downstream section have semi-gravity concrete wing wall connect to the bank slope and the earth dam.

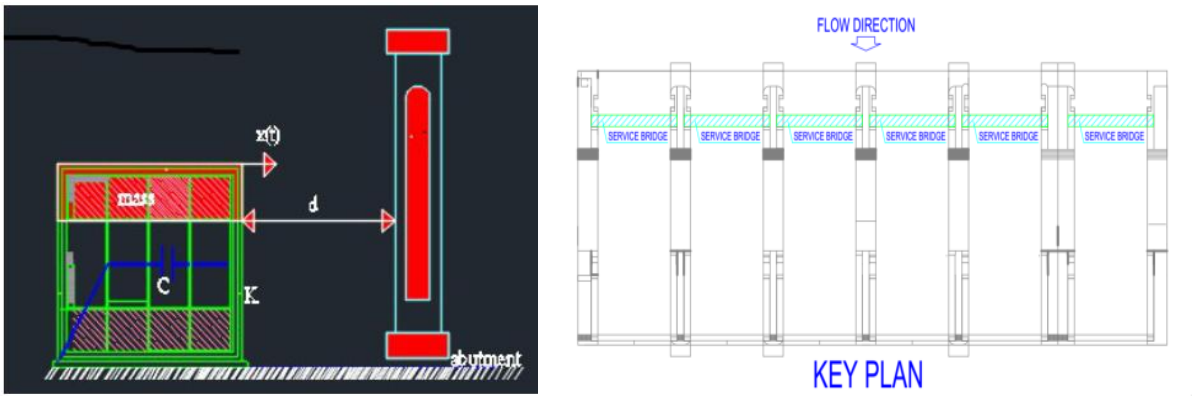

(a) (b)

Figure 3: Mechanical model of pounding interaction between structural components and schematic of simply supported bridge girders.

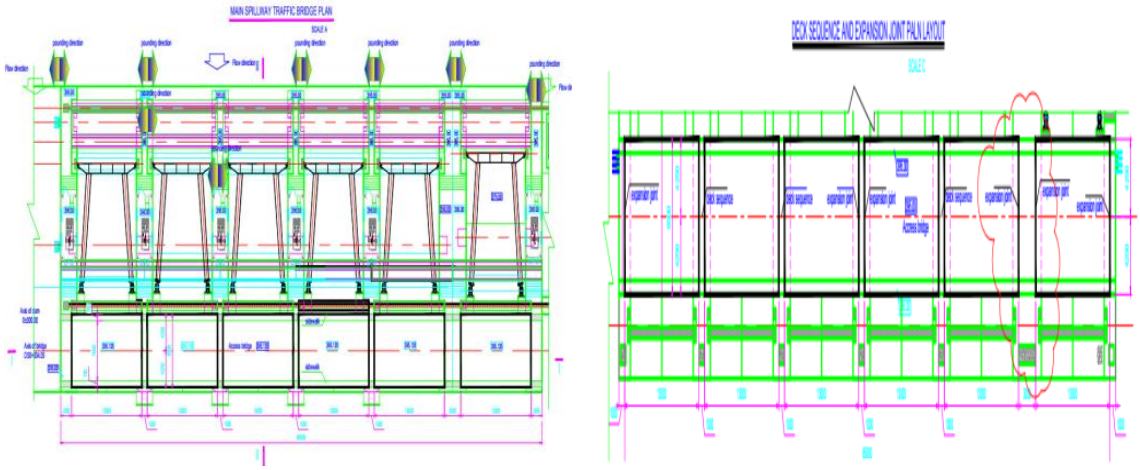

(a) (b)

Figure 4: Layout of the main spillway and flushing sluice including girder vibration scheme and expansion joint arrangement.

2.5 Structural dynamics and mathematical modeling

The earthquake excitation rotational factors implied of one torsional component, which is the rotation about the vertical axis and two rocking components defining the rotation about the two horizontal axes.

If (M) is the mass matrix, (K) is the stiffness matrix and (C) is the damping matrix, the equation of motion for structure considering a translational ground acceleration along the horizontal direction (0x) together with a rotation acceleration in the vertical plane x-z are given by: Eq. (1).

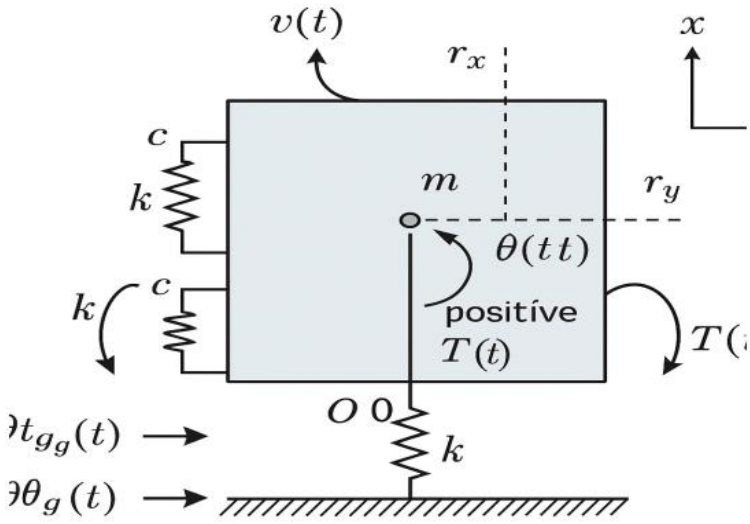

Figure 5: Diagram illustrating the three degrees of freedom of each dam component: horizontal displacements in two directions and rotation about the vertical axis.

2.5.1 Equation of motion: two-way torsionally asymmetric shear structure under seismic motions

We consider a two-way torsionally asymmetric dam-component shear structure subjected to unidirectional or bidirectional seismic motions in two orthogonal directions. Each dam component experiences three degrees of freedom: the horizontal displacements along two orthogonal axes, and a rotation about the vertical axis passing through the center of mass.

The earthquake input acceleration vectors are:

- Translational ground acceleration: $\ddot{x}_g(t)$
- Rotational ground acceleration: $\ddot{\theta}_g(t)$

The system state variables include the displacement, velocity, and acceleration vectors: $\delta(t)$, $\dot{\delta}(t)$, and $\ddot{\delta}(t)$.

Geometric and inertia properties are:

- Radius of gyration: r
- Components of radius of gyration: r_x, r_y
- Polar mass moment of inertia: J_0

The torsional stiffness k_θ and eccentricity components (e_{nx}, e_{ny}) are also considered.

The final equation of motion in matrix form is given as:

$$\begin{cases} \ddot{u}_i + 2\zeta_{ix}\omega_{ix}(\dot{u}_i - \dot{u}_g) + \omega_{ix}^2(u_i - u_g) + \omega_{ix}^2 e_{ny}\theta_i = \dfrac{F'_{nx}}{m_x} \\ \ddot{v}_i + 2\zeta_{ix}\omega_{ix}\dot{v}_i + \omega_{ix}^2 v_i - \omega_{ix}^2 e_{nx}\theta_i = \dfrac{F'_{ny}}{m_y} \\ \ddot{\theta}_i + 2\zeta_{i\theta}\omega_{ix}\dot{\theta}_i + \dfrac{m_i\omega_{ix}^2 e_{ny}}{J_0}(u_i - u_g) - \dfrac{m_i\omega_{ix}^2 e_{nx}}{J_0}v_i + \omega_{i\theta}^2\theta_i = \dfrac{T'_{n\theta}}{J_0} \end{cases} \quad (1)$$

where $i = A,B$ denotes each structural component.

Figure 5 leads the horizontal displacements along two orthogonal axes, and a rotation about the vertical axis passing through the center of mass of each dam component.

2.5.2 Extension to Three-Dimensional Excitation

The governing dynamic equation can be generalized to three-dimensional motion, where the excitation comprises six components: three translational ground accelerations, two rotational (rocking) accelerations about the horizontal axes, and one torsional acceleration about the vertical axis. Under such multidirectional loading, the equation of motion takes the following form:

$$\mathbf{M}\ddot{\boldsymbol{u}}\,(t) + \mathbf{C}\dot{\boldsymbol{u}}(t) + \mathbf{K}\mathbf{u}(t) = -\mathbf{M}\mathbf{a}_g(t) - \mathbf{M}\mathbf{R}(t) \qquad (2)$$

where:

- **M**, **C**, and **K** denote the mass, damping, and stiffness matrices, respectively,
- $\mathbf{u}(t)$, $\dot{\boldsymbol{u}}(t)$, and $\ddot{\boldsymbol{u}}\,(t)$ are the relative displacement, velocity, and acceleration vectors,
- $\mathbf{a}_g(t)$ is the ground translational acceleration vector, and
- $\mathbf{R}(t)$ accounts for the rotational acceleration components arising from rocking and torsional motions.

This formulation allows for the comprehensive analysis of structural responses under fully three-dimensional seismic or external excitation, capturing the coupling effects induced by combined translational and rotational inputs.

2.5.3 Response History Analysis

The response history analysis can be used to calculate the structural response subjected to both translational and rotational ground motion components. In this method, the response is directly computed by numerically solving Equation (2) over time. The analysis can be conducted in either linear or nonlinear regimes. Nonlinearity may arise due to:

- Material nonlinearity: variation of the stiffness matrix at each time step (e.g., yielding, cracking),
- Geometric nonlinearity: solving the dynamic equilibrium in the deformed configuration at each time step.

2.5.4 Dynamic Stability of Earth Dams

Static stability of an earth dam is typically assessed by computing a static safety factor, defined as the ratio of the soil's shear strength to the mobilized shear stress along a potential sliding surface. However, evaluating dynamic stability during an earthquake is significantly more complex. During seismic events, the pore water within the dam's soil skeleton cannot dissipate quickly, leading to the generation of excess pore water pressure. This buildup reduces the soil's effective stress and consequently decreases the shear strength, playing a crucial role in potential dam destabilization. Thus, accounting for pore pressure development is essential for accurate dynamic stability analysis of earth dams.

2.5.5 Finite Element Formulation

The dam response was simulated using the finite-element platform GeoStudio. The solution of seepage problems involving a free surface (phreatic surface) requires iterative procedures. An initial guess is refined through successive adjustments of the phreatic surface and mesh to achieve convergence of the hydraulic head H within a prescribed tolerance.

2.5.6. Darcy's Law and Governing Flow Equation

Combining Darcy's law with the conservation of mass yields the governing flow equation for transient groundwater flow:

$$\frac{\partial}{\partial x}\left(k_x \frac{\partial H}{\partial x}\right) + \frac{\partial}{\partial y}\left(k_y \frac{\partial H}{\partial y}\right) + Q = \frac{\partial \theta}{\partial t} \tag{6}$$

where:

- H is the total hydraulic head,
- k_x and k_y are the hydraulic conductivities in the x- and y-directions, respectively,
- Q is the applied boundary flux,
- θ is the volumetric water content,
- t is time.

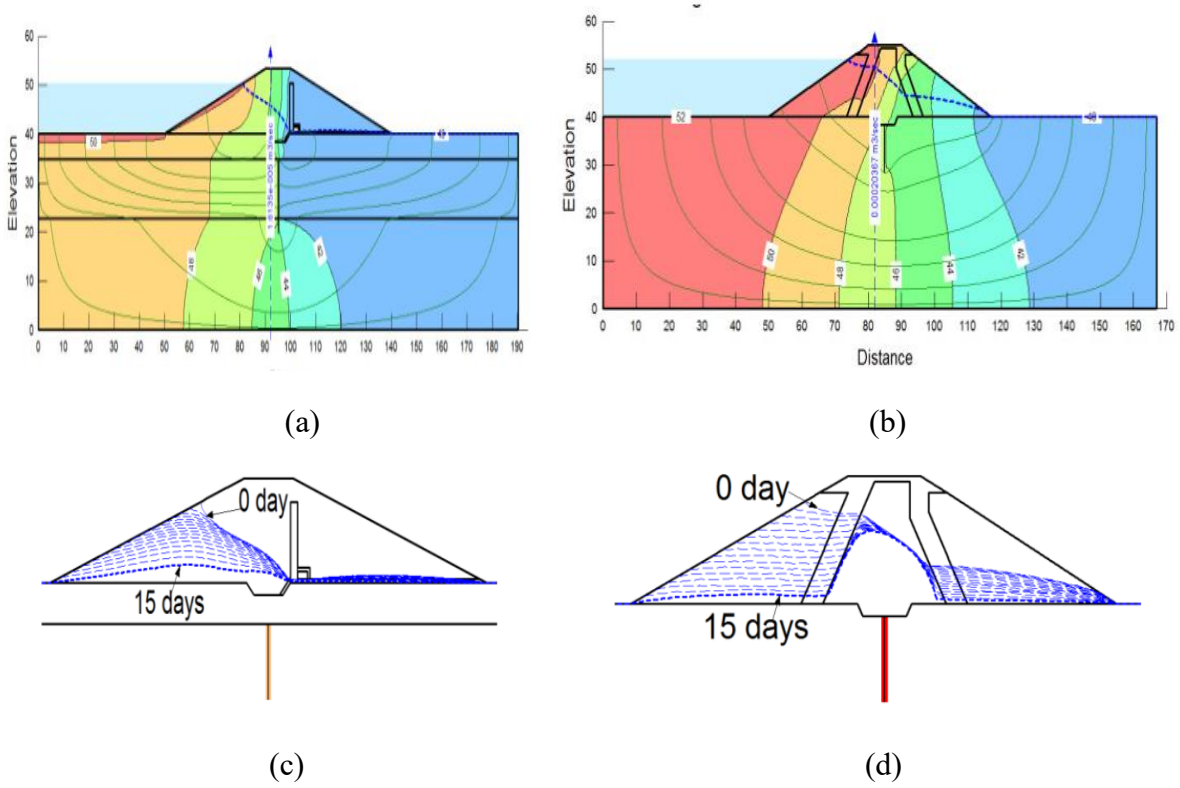

Figure 6: Flow nets and seepage lines in two sections of the embankment dam showing groundwater flow paths and phreatic surface distribution.

2.6 Seepage, Stability and Stress-Strain Analysis of the Dam

To verify the safety of the main dam, both homogeneous earth dam (section A)(zoned dam, 650m) and rock-fill dam with clay core (section B, ~ 1250m long) are considered; (see Fig. 6), where Fig. 6(a) leads Flow net for Section A and Fig. 6(c), Collection of Seepage Lines

for Section A during fifteen days of control. Fig. 6(b) shows the Flow net for Section B and the Collection of Seepage Lines for Section B during fifteen days control, Fig. 6)(d).

It is very difficult to identify discontinuities [10, 12] since some local faults may exist under thick residual soil without any ground surface traces. The discontinuities will be further mapped with progress of the follow up investigation.

Methodology used.

The measuring range of models are given: 50m extension of upstream and downstream and 40m depth of foundation. The calculation models of two sections are shown (see Fig. 6).

Besides, to indicate the variety of phreatic surfaces in draw-down condition (case1), all calculated seepage lines will be shown in one section which can be seen in Fig. 6(c); and Fig. 6(d). To conclude the method: With the water table drawing down (not shown), the unit discharge became smaller and seepage lines presented higher in the center of the dam and lower in the upstream slope and downstream slope (see Fig. 6(c); and Fig. 6(d)), which is caused by the difference of permeability coefficients between materials with different drainage conditions. It's harmful to upstream slope stability because seepage force occurred in other cases, which will not be discussed in the stability analysis in this paper. Transient seepage analysis is carried out and the emptying time of the reservoir will be used with 15 days assumed. The maximum unit discharge $0.24 * 10^{-3} m^3/s$ occurred in section B.

Calculation Content

Seepage analysis, stability and stress-strain analysis are included in the paper.

1. Purposes of seepage analysis are given as follows.
    a. To determine the location of phreatic surface and the overflow point of downstream according to the flow net.
    b. To determine the quantity of seepage of dam according to calculation.
    c. To calculate the escape or exit gradient.
2. The purpose of slope stability analysis is to get the factors of safety in all kinds of cases using the body limit equilibrium method. The pore water pressure obtained from the seepage analysis and the material attribute (shear strength) of dam is considered.
3. Stress-strain calculation can confirm settlement and stress condition of dam by increment finite element method considering constitutive models of material. It can evaluate the security of dam from another point of view.

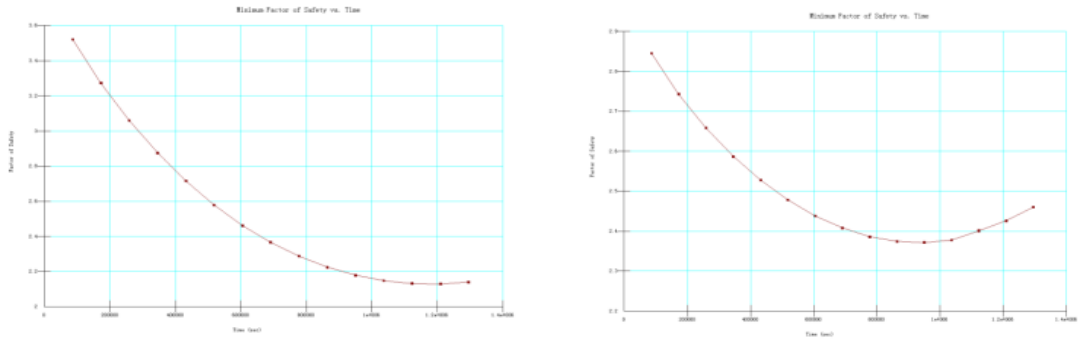

(a) (b)

Figure 7: Graphs showing variation of minimum factor of safety with time for two dam sections under transient seepage conditions.

2.7 Seepage and Hydraulic Modeling

Seepage analyses were conducted in SEEP/W under both steady-state and transient reservoir conditions. The upstream boundary was modeled as a constant head corresponding to the full reservoir level (FRL), while the downstream face was assigned a seepage exit boundary condition with toe drains. The impervious clay core and filters were explicitly modeled to evaluate their efficiency in keeping the downstream slope dry.

2.7.1 Theory of Seepage Analysis

The detail theory of seepage calculation refers to chapter 13 of Ref.[27], basic theory will be introduced in the paper. SEEP/W is formulated on the basis that the flow of water through both saturated and unsaturated soil follows Darcy's Law which states that:

$$q = k\, i \qquad (7)$$

Where: q = the specific discharge, k = the hydraulic conductivity, i = the gradient of total hydraulic head. The general governing differential equation for two-dimensional seepage can be expressed as Eq. 9.

The graph of relation between minimum Factor of safety and time can be shown in Fig.7. The zoned dam is illustrated in Fig.7(b). The shear strength related to effective stress of materials such as clay, filter and nature overburden were considered. In sensitivity analysis of slope/w modulus, all parameters will range from 0 to 1, which 0 represents minimum value and 1 represents maximum value.

2.7.2 Theory of Stress-Strain Calculation

A comprehensive explanation of the stress-strain calculation theory is provided in Chapter 15 of Ref. [26]. This section presents the fundamental concepts relevant to the present work.

SIGMA/W is a robust finite element analysis tool used to model a wide range of geotechnical stress-strain problems based on an incremental loading formulation. It is designed for two-dimensional plane strain or axisymmetric conditions and assumes small displacement and small strain theory.

The governing finite element equation used in SIGMA/W for a given time increment is expressed as:

$$\int_V [B]^T [C][B], dv, a = b \int_V \langle N \rangle^T, dv + p \int_A \langle N \rangle^T, dA + F_n \tag{8}$$

where:

A is the strain-displacement matrix, C is the constitutive matrix, *a* is the column vector of incremental nodal displacements in the xx- and yy-directions, h*N*i is the row vector of interpolation (shape) functions, A is the element boundary area, V is the element volume, b is the unit body force intensity, p is the incremental surface pressure, and F_n is the vector of concentrated incremental nodal loads.

This equation is implicitly summed over all finite elements in the domain. SIGMA/W performs incremental analysis, where at each time step, the incremental displacements resulting from incremental loads are computed and cumulatively added to those from previous steps. The output files report the total (accumulated) displacements and stresses.

It is important to note that body forces are only applied when an element becomes active for the first time during the simulation. A typical example showing the evolution of the minimum factor of safety over time is illustrated in Fig.7(a), while the corresponding zoned dam configuration is shown in Fig.7(b).

In this analysis, shear strength parameters associated with the effective stress of materials such as clay, filter materials, and natural overburden were incorporated. Additionally, a sensitivity analysis was conducted using the SLOPE/W module, wherein all input parameters were normalized to vary between 0 and 1, representing the minimum and maximum values, respectively.

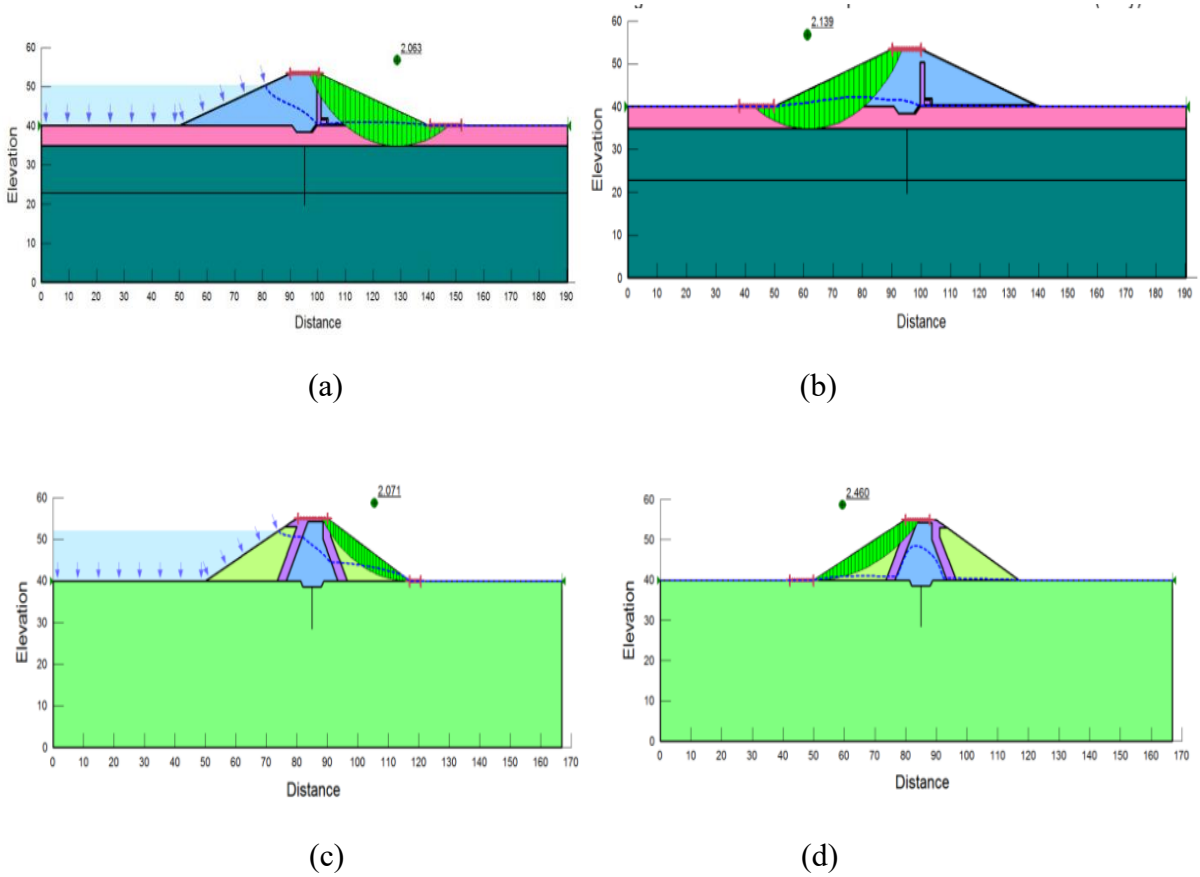

Figure 8: Critical slip surfaces and corresponding safety factors for upstream and downstream slopes of the dam.

2.7.3 Critical Slip Surface

In certain cases, not shown in this research (rapid draw-down case), the Factor of safety (Fs) of upstream slope stability decreases with time goes on Fig (7). It is reasonable that seepage force works on the upstream slope when the speed of the dropped water level is faster than the speed of pore-water pressure dissipation. The emptying time is insensitive to upstream slope stability. Besides, certain figures show that slope stability is much more sensitive to changes in overburden cohesion c (not shown).

(1). The distribution of displacement and stress is reasonable as we can see from the above contours of results.

(2). The maximum displacement on top of the dam is 0.049m occupying 0.37 percent of the height of the dam which can meet the requirement of code. This study has analyzed in 15 consecutive days, the Downstream and upstream Factors of safety and Critical Slip Surface for backfill dam fig.(8)(a) and zoned dam fig.(8)(b)

respectively. The value of critical load (greater loads during earthquakes) is mentioned with sign + in green color in fig.(8). The discontinuous blue line in each figure shows the ”Renard ”(flow failure).

Earthquakes may cause dams' liquefaction. the Flow liquefaction may arrive when the strength of the soil drops below the level needed to maintain stability under static conditions as a result of the earthquake-induced increase in pore pressure. Consequently, the static gravitational forces generate flow failures, which may conduct in large movements. Flow failures may cause the collapse of earth dams and other slopes, as well as the failure of foundations.

On zoned dam, transverse arching behavior in combinations where the geomechanical properties of the clay core (elasticity modulus and Poisson's ratio) change, provided that the material nomenclatures in the transition and shell zones are constants, fig.(9).

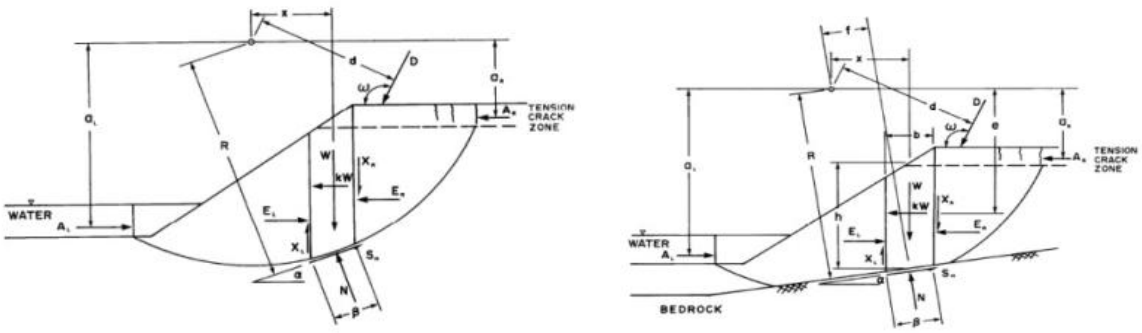

(a) (b)

Figure 9: Forces acting on slices of a sliding soil mass along circular and composite slip surfaces in slope stability analysis.

2.7.4 Theory of Stability Analysis

A detailed description of the underlying seepage theory can be found in Chapter 13 of Ref. [25], while the essential theoretical background has been briefly outlined in this paper.

SLOPE/W performs slope stability analysis using the classical limit equilibrium method, which balances forces and/or moments acting on a potential sliding mass to compute the factor of safety (FoS) against failure. The factor of safety is defined as the ratio by which the shear strength of the soil must be reduced to bring the system to a limiting equilibrium state along a specified slip surface.

In effective stress analysis, the shear strength τ_f is defined by the Mohr-Coulomb failure criterion as:

$$\tau_f = c' + \sigma' \tan \varphi' = c' + (\sigma - u) \tan \varphi' \qquad (9)$$

where:

τ_f is the shear strength, c' is the effective cohesion, is φ' the effective angle of internal friction, σ' is the total normal stress, and u is the pore water pressure.

In contrast, for a total stress analysis, the shear strength parameters are defined entirely in terms of total stresses, and pore-water pressure data are not required.

In the context of zoned earth dams, stability may also be influenced by transverse arching effects, especially when variations occur in the geomechanical properties of the clay core, such as Young's modulus and Poisson's ratio. These effects become significant while the material properties in the transition and shell zones remain constant. The interaction between zones under different stiffness conditions may result in stress redistribution and additional stability considerations, particularly under seismic or rapid draw-down conditions.

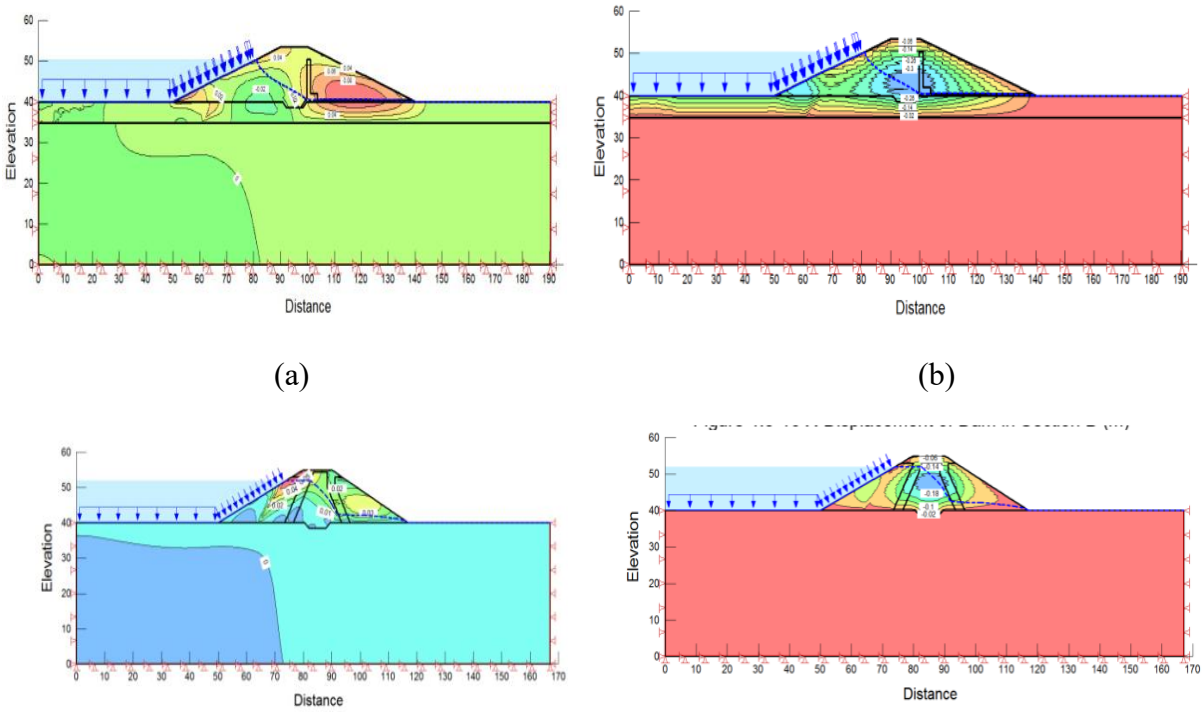

Figure 10: Contour maps showing horizontal and vertical displacement fields of the dam for two cross-sections.

2.8 Rotational forces acting on a circular and a composite slip surface

Fig. (9) shows all the forces acting on a circular and a composite slip surface of the dam. The variables are defined as shown in table. (8) in the appendix B: This table shows the horizontal seismic load applied through the centroid of each slice and all the other variables acting on dam during shaking.

The magnitude of the shear force mobilized to satisfy conditions of limiting equilibrium is:

$$S_m = \frac{s\beta}{F} = \frac{\beta(c' + (\sigma_n - u)tan\Phi)}{F} \qquad (10)$$

Where: $\sigma_n = \frac{N}{\beta}$= average normal stress at the base of each slice, F = the factor of safety, β= the base length of each slice. Reference can be made to Fig.(3) (a) and Fig.(3)(b) for deriving the moment equilibrium factor of safety equation.

Fig.(10) illustrates the displacement of the back fill dam Fig.(10)(a) and zoned dam Fig.(10) (c) in horizontal and vertical directions (see Fig.(10)(b)(d)).

2.8.1 Criteria Control

According to $EM1110-2-1901$, the critical gradient i_cr can be defined in terms of specific gravity of solids G_s and void ratio e:

$$i_c r = \frac{G_s - 1}{1 + e} \qquad (11)$$

Flotation phenomenon usually happened in soil foundation. So, escape gradient ie of section A should be checked, process of calculation can be shown in further paper.

2.8.2 Seismic Loading with Maximum Design Earthquake (0.06g)

In accordance with the relevant design codes, a maximum earthquake acceleration of 0.06g, corresponding to the Maximum Design Earthquake (MDE), is applied. The results of the analysis are presented in Table 3.

The seismic loading is characterized by a short duration, cyclic excitation involving ground motions in both horizontal and vertical directions. Such dynamic loading may induce settlement and the formation of longitudinal and transverse cracks, particularly in the vicinity of the dam crest.

Crest settlement is of particular concern, as it reduces the freeboard the vertical distance between the dam crest and the reservoir level which increases the risk of overtopping under

extreme conditions. In addition, the formation of cracks poses a critical threat to dam integrity, as they can act as preferential paths for water infiltration, potentially initiating internal erosion and piping failure, which are among the most severe forms of dam instability.

Table 3: Results of earthquakes

case	calculating section	Fs of Upstream Slope	Fs of Downstream Slope
*case*2	Section A	...	(2.28)
*case*2	Section B	...	1.41

2.8.3 maximum displacement.

The results are shown in table. (4).

Table 4: Results of displacement

section	X-displacement(m)	X-displacement (m)	Maximum displacement of
...	Upstream	Downstream	top of dam (m)
Section A	0.042	0.045	0.033
Section B	0.041	0.044	0.030

Observations from the seismic performance of earth dams during past earthquakes indicate that earthquake-induced effects are primarily associated with excessive displacements, which may arise from either instability in the absence of liquefaction or structural failure triggered by liquefaction.

Such excessive displacements occur because the dam structure is subjected to significantly greater dynamic loads during seismic events compared to those experienced under static loading conditions.

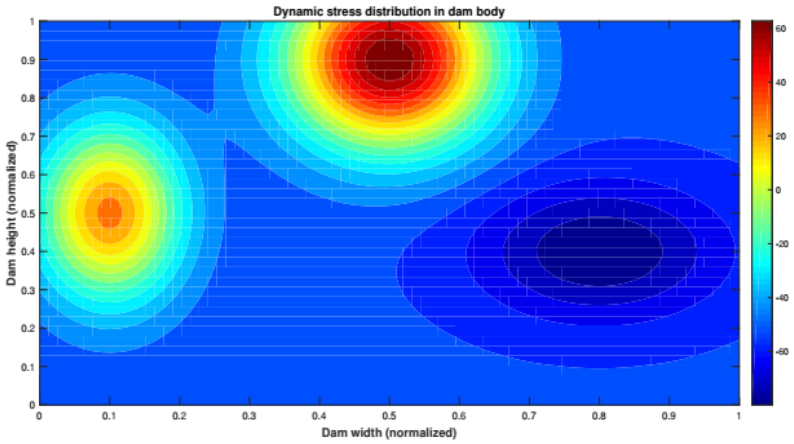

Figure 11: Stress distribution within the dam body under combined translational, rotational, and torsional seismic loading.

2.9 Seismic Response

Dynamic analyses were carried out under input ground motions decomposed into translational (u_x,u_y,u_z), rotational (θ_x, θ_y), and torsional (θ_z) components. Results highlight the following key observations:

- Displacement fields: Translational excitations primarily induced horizontal displacements in the crest region, while rotational components generated additional rocking and differential settlements between abutments. Torsional excitation was found to amplify lateral shear deformations in the shell zones, indicating sensitivity to twisting ground motion.
- Stress distribution: Figure 11 presents the stress contours in the clay core and shells. The core exhibited elevated tensile zones near the crest during rotational loading, whereas the rock-fill shells concentrated compressive stresses near the abutments. The filters functioned effectively in relieving stress concentrations at the core shell interface.
- Time-history response: Crest acceleration and displacement histories (Figure 12) revealed peak displacements of approximately 0.12 m under the design-level earthquake (PGA $\approx$ 0.15g). Rotational and torsional inputs increased crest displacements by 20-25% compared to purely translational excitation, underscoring the importance of including these components in the analysis.

Figure 12(a) shows Crest displacement time-history under translational, rotational and torsional ground motions, while, Figure 12(b) presents crest acceleration time-history.

2.10 Combined Seismic-Hydraulic Response

The coupled analysis integrated both seismic excitations and transient reservoir conditions to evaluate the dam's resilience under realistic loading scenarios. Results revealed two critical observations:

- Pore pressure response: Figure 13 shows that transient pore pressures increased within the upstream shell and clay core during shaking. While hydrodynamic pressures elevated the phreatic line temporarily, the downstream slope remained unaffected, confirming the role of the filter and drainage zones. However, localized pore pressure amplification was observed near the abutment interfaces.

- Instability zones: Combined loading induced higher shear strains near the downstream toe and at the crest, indicating potential instability zones. Safety factors computed through limit equilibrium post-processing dropped by 10-15% compared to static conditions, though remaining above the minimum recommended thresholds for embankment dams.

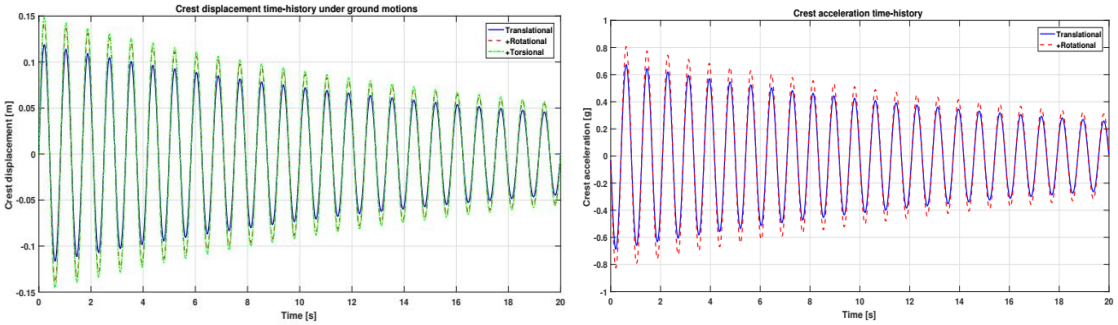

Figure 12: Time-history plots of crest displacement and acceleration under different seismic excitation components.

Overall, the integrated results highlight that while the Memve'ele dam remains stable under design-level seismic and hydraulic loads, neglecting rotational and torsional ground motion components would underestimate crest displacements and stress redistributions, potentially leading to unsafe design conclusions.

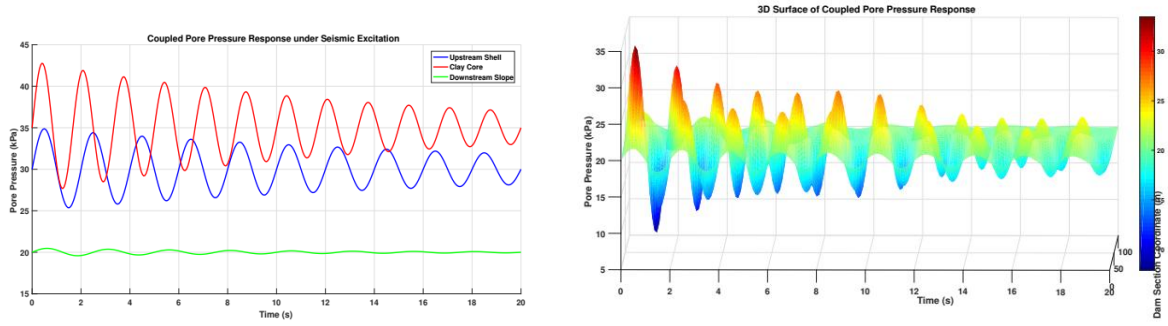

(a) (b)

Figure 13: Coupled pore pressure response in the dam body during seismic excitation under full reservoir conditions.

Figure 13(a) leads Coupled pore pressure response during seismic excitation under full reservoir condition while Figure 13(b) gives the 3d case.

Table 5 provides summary of key performance indicators of the zoned embankment dam under different loading conditions.

Table 5: Summary of key performance indicators of the zoned embankment dam under different loading conditions.

Response Metric	Static Loading	Seismic Loading	Coupled Seismic-Hydraulic
Crest horizontal displacement (m)	0.012	0.085	0.124
Crest vertical settlement (m)	0.006	0.034	0.057
Maximum pore water pressure (kPa)	95	112	148
Maximum shear stress in core (kPa)	135	265	298
Downstream slope safety factor (-)	1.85	1.32	1.08
Upstream slope safety factor (-)	2.05	1.47	1.19
Dominant crest frequency (Hz)	3.6	3.1	2.8

figure 14 highlights comparison of crest displacement, pore pressure, and downstream safety factor under static, seismic, and coupled loading scenarios while figure 15 estimated rotational components from Translational records (synthetic).

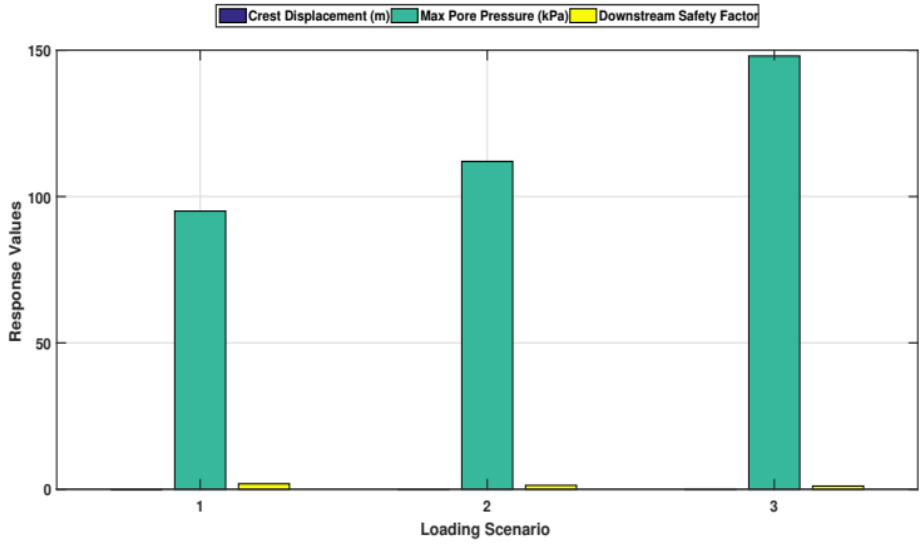

Figure 14: Comparison of crest displacement, pore pressure, and downstream safety factor under static, seismic, and coupled loading scenarios.

From figure 16 to figure 17, we provide pseudo-3D pore pressure response under Seismic Loading and coupled pore pressure response under seismic excitation respectively. figure 17(b) highlights the 3D surface, ie. coupled pore pressure response during seismic excitation. These figures combined seismic-hydraulic response, coupled pore pressure and deformation trends and critical zones of instability.

Plot equipotential lines and flow paths, Figure 1, and the figures above verify effectiveness of clay core in keeping downstream slope dry, displacement fields (translational vs. rotational vs. torsional excitation and stress distribution in core and shells.

2.11 Seismic Ground Motion Decomposition

The input seismic motions were decomposed into translational (u_x,u_y,u_z), rotational (θ_x,θ_y), and torsional (θ_z) components using finite-difference formulations derived from multi-station accelerometric records [11, 7, 6]. The rotational components were estimated as:

$$\theta_x(t) = \frac{\partial u_z}{\partial y}, \quad \theta_y(t) = -\frac{\partial u_z}{\partial x}, \quad \theta_z(t) = \frac{1}{2}\left(\frac{\partial u_y}{\partial x} - \frac{\partial u_x}{\partial y}\right), \tag{12}$$

where u_x, u_y, and u_z are translational displacements in the global coordinate system. These decomposed motions were subsequently applied as boundary excitations in the dam model.

2.12 Translational, rotational and torsional decomposition of ground motion

We adopt a rigid-body decomposition of the ground motion into three translational and three rotational components. Define an orthogonal right-handed coordinate system (x,y,z) as follows:

- x longitudinal axis (along dam axis / stream-wise);
- y transverse/out-of-plane axis (across dam axis);
- z vertical axis (positive upward).

Let $\mathbf{U}(t) = [U_x(t),\ U_y(t),\ U_z(t)]^{\mathrm{T}}$ denote the translational ground displacement time series and let $\mathbf{\Theta}(t) = [\theta_x(t),\ \theta_y(t),\ \theta_z(t)]^{\mathrm{T}}$ denote the small rotations about the x,y,z axes respectively (positive by right-hand rule). For a material point with position vector $\mathbf{r} = [x,\ y,\ z]^{\mathrm{T}}$, the rigid-body displacement imposed by the base motion is, to first order in rotation:

$$\mathbf{u}(\mathbf{r},t) = \mathbf{U}(t) + \mathbf{\Theta}(t) \times \mathbf{r}. \tag{13}$$

Writing the cross product explicitly gives the component form:

$$u_x(\mathbf{r},t) = U_x(t) + \theta_y(t)z - \theta_z(t)y, \tag{14}$$

$$u_y(\mathbf{r},t) = U_y(t) + \theta_z(t)x - \theta_x(t)z, \tag{15}$$

$$u_z(\mathbf{r},t) = U_z(t) + \theta_x(t)y - \theta_y(t)x. \tag{16}$$

The angular velocities (if needed for inertia terms) are the time derivatives:

$$\omega(t) = \dot{\theta}(t). \tag{17}$$

Relation between rotation field and spatial gradients of translational motion

For a continuous displacement field $\mathbf{u}(\mathbf{r},t)$, the infinitesimal rotation tensor (vector) may be expressed in terms of spatial derivatives of the translational field via the (vectorial) curl:

$$\boldsymbol{\Theta}(\mathbf{r},t) = \tfrac{1}{2}\nabla \times \mathbf{u}(\mathbf{r},t) \quad \Longrightarrow \quad \begin{cases} \theta_x = \frac{1}{2}\left(\frac{\partial u_z}{\partial y} - \frac{\partial u_y}{\partial z}\right) \\ \theta_y = \frac{1}{2}\left(\frac{\partial u_x}{\partial z} - \frac{\partial u_z}{\partial x}\right), \\ \theta_z = \frac{1}{2}\left(\frac{\partial u_y}{\partial x} - \frac{\partial u_x}{\partial y}\right). \end{cases} \tag{18}$$

This relation is exact for a continuous displacement field and can be used to estimate rotations from spatially distributed translational records (measured at multiple stations) or from analytic/plane wave approximations of the seismic field.

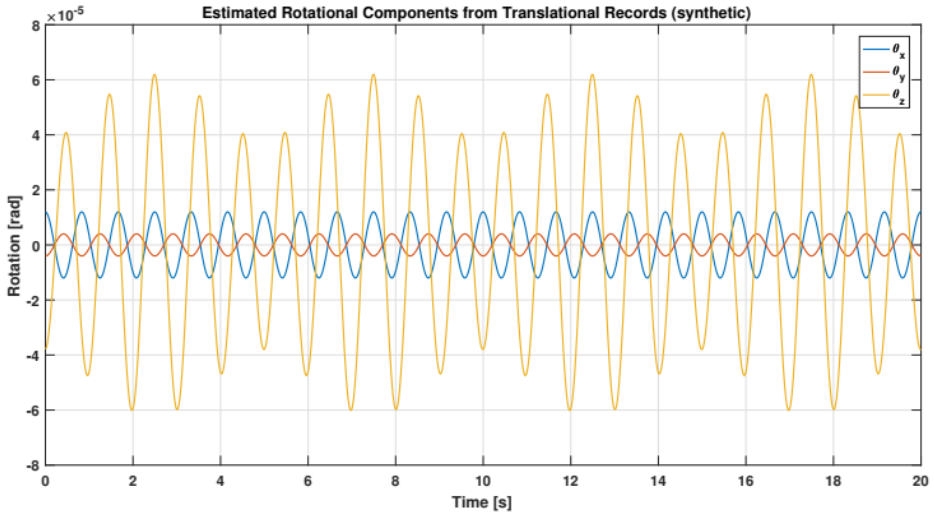

Figure 15: Estimated Rotational Components from Translational Records (synthetic)

Practical implementation for Geo-Studio (pseudo-3D via multiple 2D sections)

Geo-Studio (SEEP/W, SLOPE/W, SIGMA/W) is inherently 2D. To capture 3D translational and rotational effects in a pseudo-3D manner we recommend the following practical procedure:

1. Select a set of 2D cross sections along the dam axis at distinct transverse coordinates $y = y_j$ ($j = 1...N$). Each cross-section is modeled in Geo-Studio as an independent 2D plane (x,z) slice located at y_j.
2. Prepare base translational time series $\mathbf{U}(t) = [U_x(t), U_y(t), U_z(t)]$ either from recorded motions or scaled synthetic records.
3. Obtain or estimate rotational time series $\boldsymbol{\Theta}(t) = [\theta_x(t), \theta_y(t), \theta_z(t)]$:

- use direct rotational records if available, or
- estimate rotations from spatial gradients of translations (Equation 21) using dense station data, or
- compute rotations from plane-wave approximations or theoretical relations (document assumptions clearly).

4. Apply combined displacement to base nodes of each 2D section. For the 2D slice at $y = y_j$ set the base displacement time-histories for a base node at (x_b,y_j,z_b) via Equations 17–19.

In practice the *x*- and *z*-components applied in the 2D model are:

$$u_x^{\text{base}}(t; y_j) = U_x(t) \; + \; \theta_y(t)\, z_b \; - \; \theta_z(t)\, y_j,$$

$$u_z^{\text{base}}(t; y_j) = U_z(t) \; + \; \theta_x(t)\, y_j \; - \; \theta_y(t)\, x_b,$$

where x_b and z_b are the coordinates of the base node in the local 2D slice (choose x_b consistent across sections).

5. Run each 2D dynamic analysis independently in GeoStudio with its section-specific base histories. Post-process the ensemble of 2D results to reconstruct along-axis (3D) variations in response (displacement, pore-pressure, stress).

Notes and caveats

- The rigid-body formula eq.16 assumes *small* rotations (typical in engineering seismic applications). For large rotations higher-order terms would be required.
- The accuracy of pseudo-3D results depends on the number of 2D slices, the spatial sampling along *y*, and the validity of the assumed rotational time histories. Always document how rotations were obtained and quantify uncertainties.
- When rotations are not directly measured, show sensitivity runs (e.g., ±20-50% in θ amplitudes) to demonstrate robustness of conclusions.

figure 18; (Workflow for coupling Geo-Studio (2D FE models) with MATLAB routines to achieve a pseudo-3D seismic-hydraulic analysis of the Memve'ele Dam.) confirms the result above.

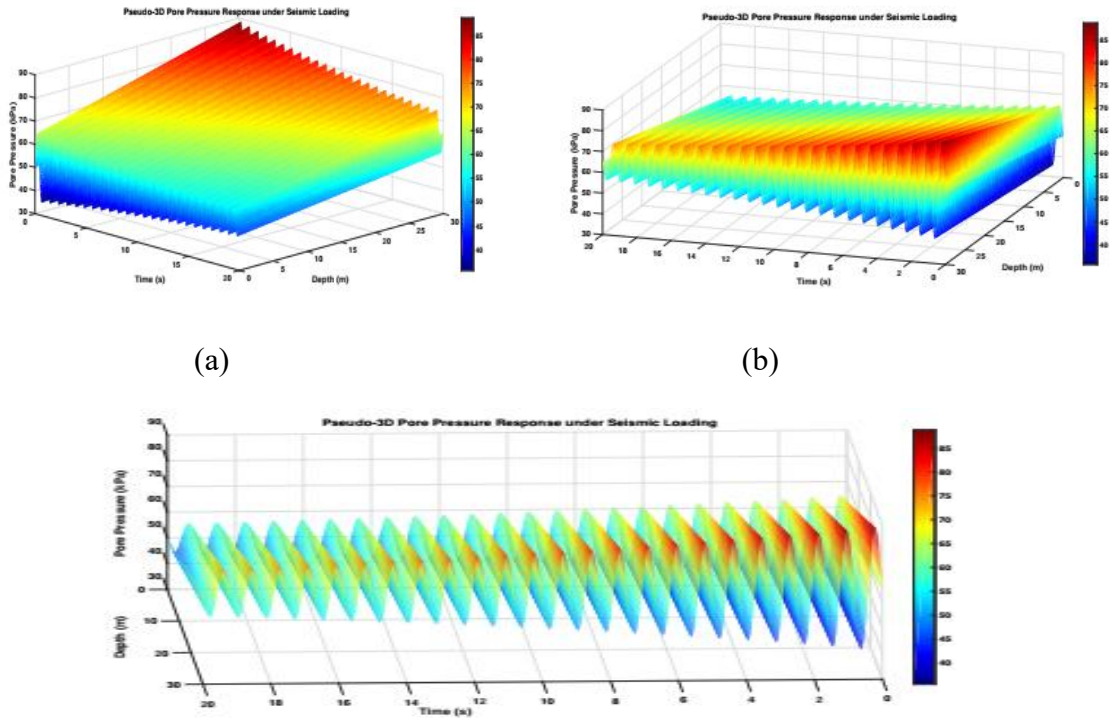

Figure 16: Pseudo-3D Pore Pressure Response under Seismic Loading

2.13 Coupling Geo-Studio with MATLAB (Pseudo-3D Approximation)

Since Geo-Studio is inherently a two-dimensional tool, a hybrid coupling framework was developed to approximate three-dimensional effects. The approach involved:

1. Extracting multiple 2D cross-sections of the dam (central section, left abutment, right abutment) for independent analysis in SLOPE/W and QUAKE/W.
2. Implementing MATLAB routines to process seismic records, compute rotational/torsional components, and scale them for input into each 2D slice.
3. Applying equivalent stress correction factors to capture out-of-plane effects in a pseudo-3D manner.

A flowchart of the integrated GeoStudio-MATLAB framework is presented in Figure 16, ensuring methodological transparency and addressing concern regarding the feasibility of 3D analyses with GeoStudio 2007.

2.14 Numerical Simulation Setup

Three sets of simulations were performed:

- Static analysis: dam self-weight and hydrostatic reservoir pressure.

- Seepage analysis: steady and transient reservoir fluctuations with phreatic line evaluation.
- Seismic analysis: input ground motion records (translational + rotational/torsional) applied under normal and flood conditions.

Dynamic input was scaled according to regional seismic hazard levels for southern Cameroon (PGA ≈ 0.15g), with hydrological loading corresponding to the 100-year flood level. This combined loading framework allows for an integrated assessment of structural stability, seepage performance, and seismic resilience.

2.15 Application of Decomposed Motions to a 2D GeoStudio Slice

For a 2D vertical slice of width L at abscissa x_s (measured from the reference station), the input acceleration field is obtained by superposing translational, rotational, and torsional components. Denoting the horizontal (u), vertical (v), and out-of-plane (w) translational accelerations as $\ddot{u}_g(t)$, $\ddot{v}_g(t)$, and $\ddot{w}_g(t)$, and the rotational rates as $\ddot{\theta}_x(t)$, $\ddot{\theta}_y(t)$, $\ddot{\theta}_z(t)$, the effective nodal acceleration at slice coordinate z is:

$$\ddot{U}_s(t) = \ddot{u}_g(t) + \ddot{\theta}_z(t)(z - z_0) - \ddot{\theta}_y(t)(x_s - x_0), \tag{19}$$

where:

- (x_0, z_0) is the reference point (e.g., centroid of the slice base),
- $\ddot{\theta}_z(t)$ represents torsional excitation about the vertical axis,
- $\ddot{\theta}_y(t)$ represents rocking motion about the out-of-plane axis.

For the vertical degree of freedom at the same slice, the coupled input becomes

$$\ddot{V}_s(t) = \ddot{v}_g(t) + \ddot{\theta}_x(t)(z - z_0), \tag{20}$$

Where $\ddot{\theta}_x(t)$ denotes rocking about the in-plane horizontal axis.

Thus, each 2D slice in GeoStudio is driven by a composite input that accounts for both the base translational accelerations and the differential contributions from rotation and torsion, ensuring kinematic compatibility with the full 3D ground motion field.

3. Results

Seepage and stress analyses were performed using the finite-element platform GeoStudio, coupled with MATLAB routines for seismic loading decomposition.

3.1 Engineering Application: Constitutive model for the backfill

The inelastic reactions, and frictional contact of Soil combined with gapping between the soil and the foundation elements are given.

Fig.19 gives the force and displacement reactions of a 45-degree skew wall under a cyclic displacement and rotation combination load. Fig.19(a) shows Force reaction of finite element modeling (FEM). Therefore, Fig.19(b) leads the motion of finite element modeling due to external excitation.

3.2 Gradation design investigation of filter, transition and rock-fill of clay core rock-fill dam

The filter design for the rockfill dam with clay core experiences a critical part of the embankment design. It is essential that the individual particles in the foundation and embankment are held in place and do not move as a consequence of seepage force. This is accomplished by ensuring that the zone of material meets filter criteria concerning adjacent materials. In the zoned embankment, the coarseness between the fine and coarse zones may be such that an intermediated or transition section is required.

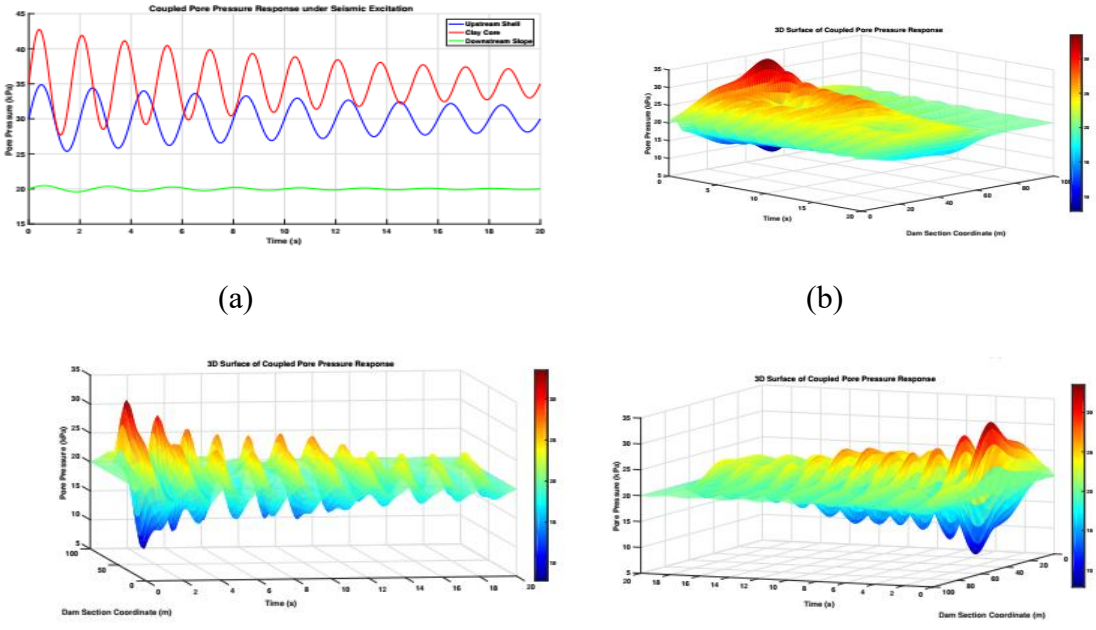

(a) (b)

(c) (d)

Figure 17: Two-panel figure illustrating pore-water pressure response during seismic loading. Panel (a) shows the temporal or spatial distribution of coupled pore pressure within the dam body under seismic excitation. Panel (b) presents a three-dimensional surface plot visualizing variations in pore pressure magnitude across the modeled domain.

The present pseudo-3D approach approximates spatial seismic variability using multiple two-dimensional slices. Although computationally efficient, the approach cannot fully reproduce complex three-dimensional wave propagation effects.

3.3 The spillway and their appurtenant structures

The rotational slip and stick condition of the bridge segments at their points of contact are related to the components of the joint segments' tendency to rotate, which can lead to detachment. The initial exploration of the pier^{0}s or spillway^{0}s seismic behavior was conducted using a Geo-studio FE response shown in Fig.20. This analysis utilized linear material properties and uncracked stiffness. The results indicated that the pier will experience significant seismic deformations at the top, with its moment capacity falling short of the seismic demand. Consequently, the pier will likely fail in flexure. Considering the under-reinforced nature of the pier, the tensile reinforcement is expected to fracture, as illustrated in Fig.20(a). The cracking may progress through the pier's entire thickness, leading to detachment.

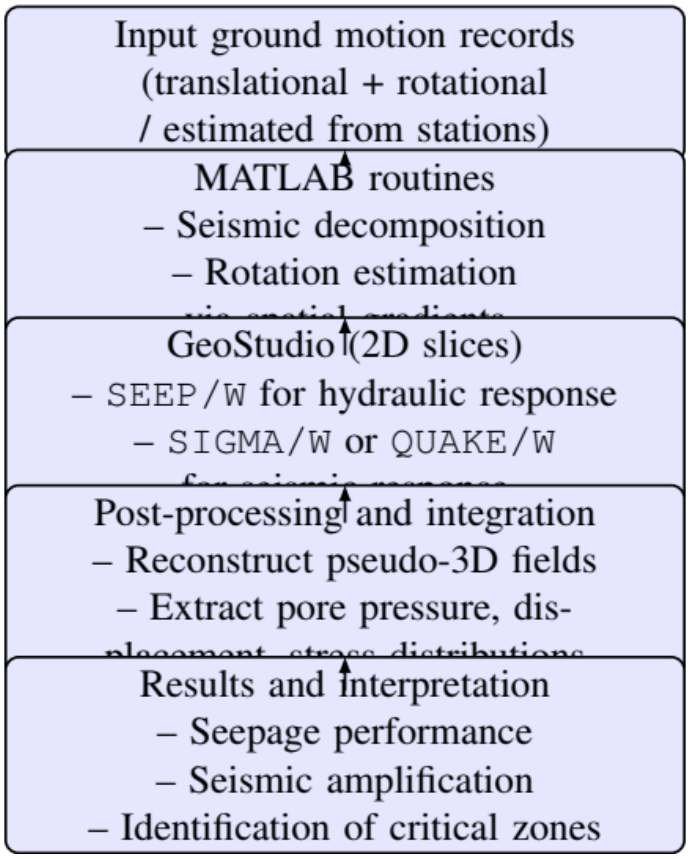

Figure 18: Flowchart diagram showing the workflow for coupling GeoStudio two-dimensional finite-element models with MATLAB computational routines to perform pseudo-three-dimensional seismic-hydraulic analysis of the Memve'ele embankment dam.

The analysis focuses on the main spillway's stability under various loading scenarios. It primarily assesses sliding stability, overturning stability, and foundation stress. For this spillway, calculations incorporate both the standard central pier and side pier monoliths. The stability assessment utilizes the monolith width for both main and side piers. Refer to the detailed drawing in Fig.25 in appendix C.

Figure 21 shows the force and displacement reactions of a 45-degree skew wall subjected to a cyclic displacement and rotation load. Figure 21(a) presents the force and moment reactions of this wall under the same cyclic combination of displacement and rotation (displacement versus rotation). Figure 21(b) depicts the relationship between the bridge's rotation (in radians) and moment (displacement).

NB. See more details of safety and stability of dam components in appendix B.

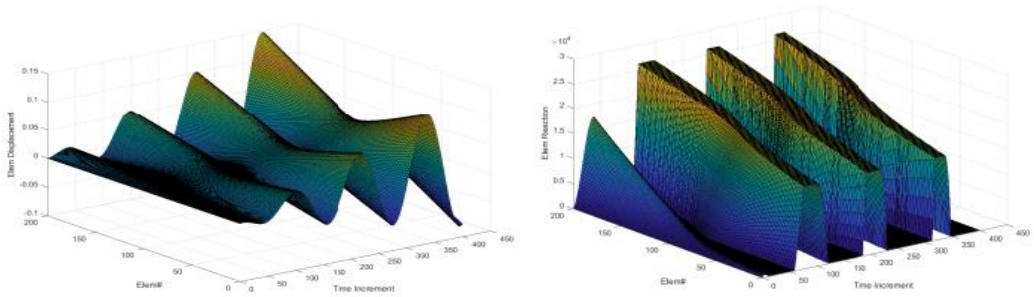

Figure 19: Two-panel plot of finite-element simulation results for a 45-degree skew wall subjected to cyclic displacement and rotational loading. Panel (a) displays the force reaction response, while panel (b) illustrates the resulting displacement or motion behavior of the wall under external excitation.

The reservoir will be impounded to a level of 392m, creating a pond of about 13 km long and covering an area of 19km^2, amongst which 12km^2 land will be submerged.

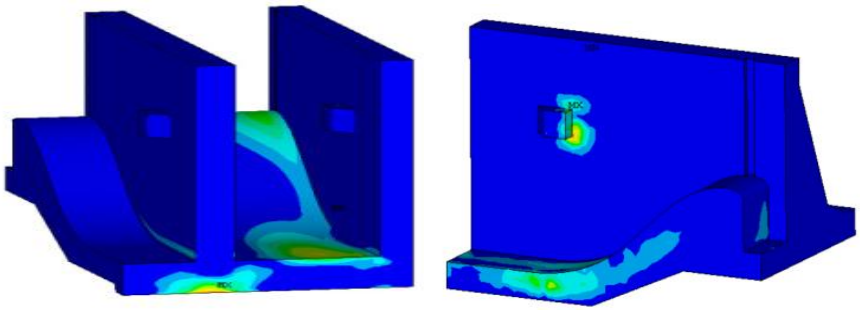

(a) (b)

Figure 20: Stability analysis results for the main spillway structure under different loading conditions, showing the structural configuration and response of a typical middle pier section.

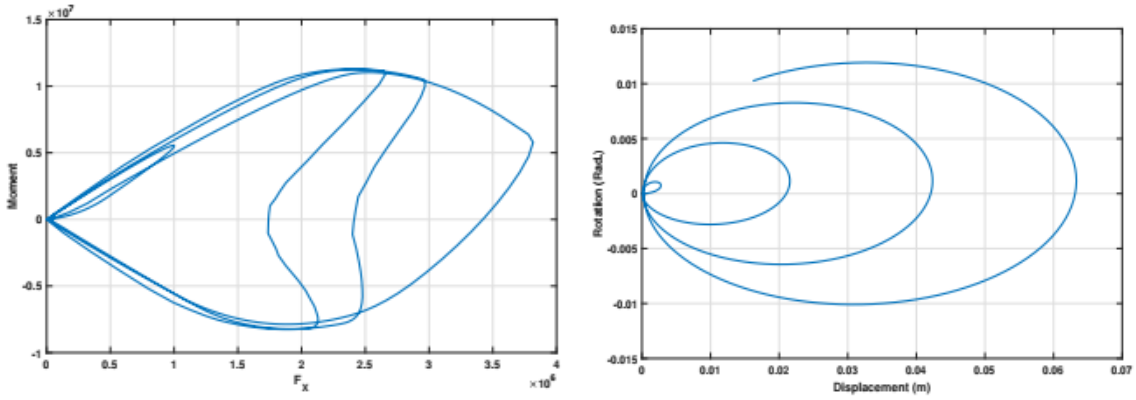

(a) (b)

Figure 21: Graphs illustrating the mechanical response of a 45-degree skew wall subjected to cyclic displacement and rotation. The plots show the relationship between displacement, rotation, and the resulting force or moment reactions derived from numerical modeling.

4.2.1 Selected ground motion

The ground motion records in (0x)- and (0y)-direction of the 1989 Cameroon earthquake are selected to illustrate the provided strategy with alternative analysis options. The records' PGA is scaled to 0.4g in both directions.

The two components of the chosen ground motion are not shown, together with their respective acceleration, velocity, and displacement time histories.

These records have a duration of approximately 30 sec and a time step size of 0.005 s.

Table 6 gives Local earthquakes and strong events felt in southern Cameroon; ie. seismic pounding of this century correlate with Congo craton/mobile zone border.

Table 6: Local earthquakes and strong events felt in southern Cameroon: seismic pounding of this century correlate with Congo craton/mobile zone border

Date	time	Magnitude	Latitude (degrees)	Longitude (degrees)	Depth(Km)	(I:Intensity in ISC scale)
1903 June 10	...	4.4	(3*N*10.0*E*)	....	79.4	3.7
1911 March 26	...	5.7	3.1*N*11*E*	...	119.3	4.6
1913 October 9	...	5.1	3.8*N*12.3*E*	...	280.0	1.6
18/08/87	10 : 42	2.6	...	...	...	... (...)
04/09/87	21 : 30	4.0	3*N*10.31	9*E*50.92	30	5.5

11/09/87	04 : 11	3.7	3*N*08.82	10*E*08.01	...	...
17/09/87	14 : 09	3.3	3*N*01.70	10*E*02.34	...	...
18/09/87	11 : 04	2.8	3*N*47.16	10*E*20.95	27	3.9
19/03/88	13 : 10	3.4	3*N*30.09	9*E*53.95	65	2.7
14/03/89	15 : 24	2.8	4*N*02.1	11*E*23.46	...	... ...
16/03/89	13 : 19	3.5	2*N*59.34	9*E*43.97	...	... ...

4.2.2 pounding phenomenon observed through the mobile zone/Congo craton margin of Central Africa

Figure 22 shows the magnitude and recorded peak acceleration in relation to the distance to the earthquake epicenters, as well as the peak acceleration in relation to the amplitude of the earthquake. The acceleration values are the absolute maximum values for each direction (south-west to north-west) retrieved from the time series. The depicted values represent peak ground acceleration recorded in the structure's basement. These values do not represent a total horizontal acceleration component, but the highest value of both sensors recording in the south-west and the highest value of the north-west sensor. It should be noted that both of those peak values of acceleration are not expected to occur at the same time. Figure 22 depicts historical peak ground acceleration. Fig.22(a) depicts the earthquake magnitude in relation to the distance to the epicenters, whereas Fig.22(b) depicts the peak acceleration in relation to the distance to the epicenters and Fig.22(c) represents the peak acceleration in relation to the earthquake magnitude. The dots show maximum horizontal acceleration.

5. Discussion

The numerical results presented in this study provide new insights into the hydro-seismic safety of the Memve'ele zoned embankment dam under static, seismic, and coupled seismic-hydraulic conditions. By integrating seepage analyses with dynamic ground motion decomposition, this work builds upon and extends the growing body of literature addressing the seismic response of embankment dams. For instance, studies by Ambraseys and Sarma (1967) and Seed et al. (1978) emphasized the importance of accounting for pore pressure buildup and nonlinear soil behavior in seismic stability assessments, while more recent work by Gazetas et al. (2004) and Yacoub et al. (2015) demonstrated the role of finite element

modeling in resolving stress redistribution within zoned dams. Compared with these prior investigations, the present study explicitly incorporates rotational and torsional ground motion components, which have generally been overlooked in African case studies, despite their potential significance for wide-crested earth structures.

The results indicate that while the clay core successfully limits seepage under static conditions, seismic loading induces noticeable redistribution of pore pressures, particularly under coupled hydro-seismic excitation. This observation is consistent with findings reported by Chwang and Housner (1970) and Liu et al. (2012), who noted that dynamic pore pressure amplification can substantially reduce the effective stress and safety margin of embankment dams. Furthermore, the computed safety factor of 1.08 under coupled loading approaches the threshold of instability, echoing concerns raised in studies of other African earth dams where construction materials, monitoring infrastructure, and design methodologies may not fully account for complex seismic hazards.

Despite these contributions, several methodological limitations must be acknowledged. The use of a pseudo-3D approximation linking two-dimensional Geo-Studio analyses with MATLAB based decomposition of ground motion cannot capture all three-dimensional stress redistributions or failure mechanisms. Effects such as longitudinal cracking, arching between abutments, and non-uniform reservoir impoundment are only approximated through correction factors or multiple 2D sections. While this hybrid method provides a pragmatic compromise given computational constraints and limited regional seismic records, full 3D nonlinear dynamic analyses would provide more definitive insights, particularly for dams with irregular geometry or heterogeneous zoning. Another limitation lies in the assumption of homogenous material properties within each zone, whereas natural variability in permeability, density, or stiffness could significantly influence local pore pressure gradients and failure modes.

From a practical perspective, the findings underscore the necessity of revisiting dam design and safety evaluation practices in Africa, where most embankment dams have historically been assessed using simplified static or 2D methods. The inclusion of rotational seismic components reveals that safety margins may be narrower than previously assumed, suggesting the need for both updated design codes and improved site-specific investigations. For new projects, these results recommend adopting more rigorous seismic hazard assessments that integrate both translational and rotational motion. For existing dams, targeted reinforcement of critical zones, such as the downstream shell or core shell interfaces, may enhance resilience under combined seismic-hydraulic loading. In broader terms, this study

highlights the importance of coupling advanced numerical modeling with pragmatic field validation to inform the sustainable management of large dams across the African continent.

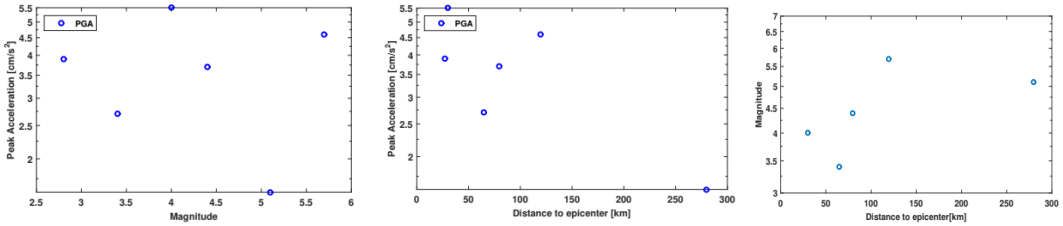

(a) (b) (c)

Figure 22: ***Three scatter plots presenting historical peak ground acceleration data. Panel (a) relates earthquake magnitude to distance from the epicenter, panel (b) shows peak acceleration versus distance to the epicenter, and panel (c) shows peak acceleration versus earthquake magnitude.***

6. Case Studies: Experimental, Numerical Results and discussion

Several layout scenarios are also studied, including one or more weak buildings, such as the earth dam, next to a stiffer building (abutment). As a result of the differing dynamic properties, the pounding of neighboring components consists of impacts at various levels. The repeated impulsive actions have extra internal consequences that are taken into account in this work. The numerical data is compared based on forces, collision time, and total transmitted momentum. Finally, alternative configurations of these structures with varying dynamic properties are presented and tested.

6.1 Numerical simulation of the system

Six coupled second-order differential equations are numerically integrated using the fourth-order Runge-Kutta scheme with an adaptive step size control to solve the system of differential equations.

ie. $y = \{x_A, \dot{x}_A, y_A, \dot{y}_A, \theta_A, \dot{\theta}_A, x_B, \dot{x}_B, y_B, \dot{y}_B, \theta_B, \dot{\theta}_B\}^{'}$, the symbol $^{'}$ defines the $^{-}$ transpose of vector. The above systems of adjacent dam components are reorganized as a set of 12 first-order differential equations as $\dot{y} = f(t,y)$. The initial values $y(t_0) = y$ are denoting the initial motions and velocities of the structure. The allowable error in the iterations was set to 0.1 percent. The initial time step was set by the Fortran program automatically, typically in the order of 0.01, consequently, this changed with the current values of the first derivatives of the displacement variables. Unless otherwise specified, the numerical values are given as $\alpha_A = 15^{\circ}$; $\alpha_B = 17^{\circ}$; MA=1.2M_B ; $f_A = 2.54$Hz ; $f_B = 2.83$Hz ; $f = 2.50Hz$; $a = 0.5$m ; $\zeta_{Ax} = \zeta_{Ao} = 0.052$; ζ_{Bx}

$= \zeta_{Bo} = 0.047$; $e_{Ay} = -112$mm; $e_{By} = 70$mm. With f_A, f_B the natural frequencies of the component, and f the natural frequency of the seismic wave.

This section is particularly important to highlight semantic terms. Therefore, the terms ground acceleration and velocity are often related to the translational component of acceleration and velocity only. The translational acceleration and the translational velocity are given to distinguish these components from the rotational acceleration and rotational velocity, respectively (see Fig. 23 to Fig. 24). Accordingly, average rotation is a good choice because chord rotation is often sensitive to gap distance, so the point rotation doesn't take into account the presence of a foundation. Computing dynamic strains in soil and estimating rotational components of ground motion as shown in Fig. 23 with site-specific characteristics, including the apparent seismic wave velocity and the frequency content of expected ground motions, is provided. Fig. 23(a) and Fig. 23(b) highlighted the rotation and bifurcations that occur during particle motion and their phase portrait rotation in vertical displacement, respectively. The chaotic behavior is observed in the center of the structure and could accelerate his failure. Fig. 23(c) provides in 3 dimensions the rotation versus speed in the vertical axis (torsion). The drawdown is inevitable for the frame structure mechanics model from phase portrait rotation Fig. 23(d) in oy (rotation in the vertical axis inside the dam) to Fig. 23(d): phase portrait in x-z: rotation in the vertical axis inside the dam. Fig. 23(e) leads to torsion versus time. The catastrophic case is when the particle turns round, as observed in Fig. 23(d).

Fig. 24(a) represents the 3-D rotation of particles and bifurcation. Therefore, Fig. 24(b) provides the phase portrait: the speed versus displacement in horizontal displacement. Fig. 24(c) shows in oy (vertical displacement).

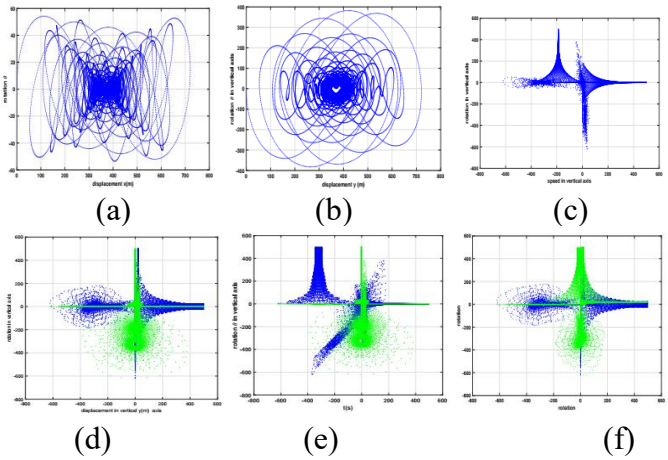

Figure 23: Conceptual mechanical model of a frame structure. Panel (a) illustrates rotational motion within the structural system, and panel (b) presents a phase portrait showing vertical rotational dynamics of the system.

6.2 Table: Comparison of Key Features Between Previous Studies and This Research

Table 7 presents comparison of previous studies and the present work.

Feature	Previous Studies	This Study
Seismic Loading Dimension	1D or 2D horizontal ground motion	Full 3D motion: translational + rotational components
Hydraulic Loading Consideration	Often simplified or steady-state seepage only	Time-dependent seepage with transient pore pressure analysis
Material Model	Homogeneous or simplified zonation	Realistic zoned embankment with material heterogeneity
Stress-Strain Analysis	Linear-elastic or limit equilibrium only	Nonlinear FEM analysis using SIGMA/W under small strain theory
Stability Evaluation Method	Classical limit equilibrium methods	Coupled FEM + limit equilibrium using stress update from FEM
Failure Modes Considered	Global slip surfaces; often neglect cracking	Includes crest settlement, transverse cracking, and overtopping potential
Dynamic Pore Pressure Effects	Neglected or approximated	Modeled through effective stress and excess pore pressure evolution
Sensitivity Analysis	Limited to one or two parameters	Multi-parameter sensitivity: modulus, cohesion, angle of friction, etc.
Application	Generic dam models or simplified geometry	Real-world case study: Memve'ele Hydroelectric Project

6.2 Table: Comparison of Key Features Between Previous Studies and This Research

Table 7 presents comparison of previous studies and the present work.

Feature	Previous Studies	This Study
Seismic Loading Dimension	1D or 2D horizontal ground motion	Full 3D motion: translational + rotational components
Hydraulic Loading Consideration	Often simplified or steady-state seepage only	Time-dependent seepage with transient pore pressure analysis
Material Model	Homogeneous or simplified zonation	Realistic zoned embankment with material heterogeneity
Stress-Strain Analysis	Linear-elastic or limit equilibrium only	Nonlinear FEM analysis using SIGMA/W under small strain theory
Stability Evaluation Method	Classical limit equilibrium methods	Coupled FEM + limit equilibrium using stress update from FEM
Failure Modes Considered	Global slip surfaces; often neglect cracking	Includes crest settlement, transverse cracking, and overtopping potential
Dynamic Pore Pressure Effects	Neglected or approximated	Modeled through effective stress and excess pore pressure evolution
Sensitivity Analysis	Limited to one or two parameters	Multi-parameter sensitivity: modulus, cohesion, angle of friction, etc.
Application	Generic dam models or simplified geometry	Real-world case study: Memve'ele Hydroelectric Project

6.3 Unique Contributions of the Study

This study presents a comprehensive structural integrity analysis of zoned embankment dams subjected to combined seismic and hydraulic loading, using the Memve'ele Hydroelectric Project as a representative case study. The key contributions of this research include the integration of multi-dimensional ground motion inputs-encompassing three translational and three rotational acceleration components into the dam stability framework. Unlike conventional approaches that consider simplified or uniaxial seismic excitation, this study employs a fully three dimensional dynamic model to capture realistic loading conditions. Additionally, the analysis incorporates time-dependent consolidation effects, effective stress based shear strength formulations, and spatially variable material properties to enhance the reliability of factor of safety predictions.

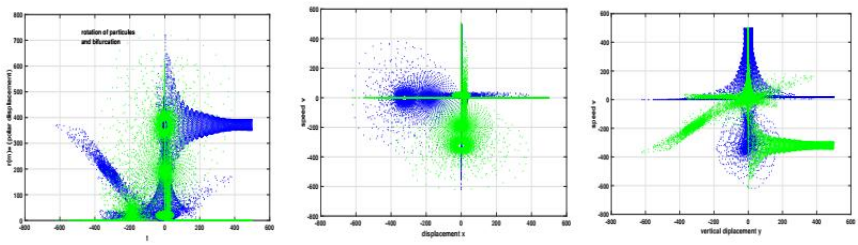

(a) *(b)* *(c)*

Figure 24: Mechanical model of frame structure dynamics showing particle rotation and bifurcation behavior. Panel (a) illustrates rotational motion and bifurcation patterns, while panel (b) presents the corresponding phase-space representation.

A novel Table 7: Comparison of Previous Studies and the Present Work analytical framework has been developed by coupling finite element stress-strain simulations (via SIGMA/W) with advanced limit equilibrium stability evaluations (using SLOPE/W), enabling dynamic updates of internal stresses and pore pressures throughout the loading history. This integrated methodology allows for the assessment of critical failure mechanisms, such as crest settlement, transverse cracking, and potential overtopping under seismic conditions. The study also introduces a sensitivity analysis scheme that systematically quantifies the influence of geomechanical parameters such as cohesion, internal friction angle, and modulus of elasticity on slope stability, thereby offering a robust tool for seismic risk informed dam design.

7. Conclusions and Recommendations

This study investigated the hydro-seismic safety of the Memve'ele embankment dam through an integrated methodology combining two-dimensional finite element modeling in

Geo-Studio with MATLAB-based decomposition of seismic ground motion into translational, rotational, and torsional components. The main findings can be summarized as follows:

1. Parameter sensitivity: The reliability of dam safety assessments is highly dependent on the careful selection of soil and hydraulic parameters. The analysis demonstrated that small variations in shear strength parameters or permeability values significantly influence both seepage behavior and slope stability. This underlines the necessity of using site-specific geotechnical investigations, supplemented by laboratory and field tests, rather than relying on generic assumptions.
2. Influence of rotational and torsional seismic effects: While traditional analyses focus on translational ground accelerations, the present study shows that rotational and torsional components can amplify crest displacements, stress redistribution, and pore pressure variations. This finding reinforces the need to adopt a more comprehensive seismic hazard framework for embankment dams, particularly in African contexts where seismic design guidelines remain limited.
3. Seepage control and the role of the clay core: The clay core was effective in limiting downstream seepage under static conditions, but under combined seismic-hydraulic loading, localized increases in pore pressure were observed. These results highlight the importance of verifying seepage control measures under both static and dynamic scenarios, ensuring that filter and drainage systems are designed with sufficient redundancy.

Beyond these technical findings, the study offers several practical recommendations:

- Monitoring strategies: Long-term monitoring of pore water pressures, crest displacements, and internal deformations should be incorporated into dam safety management programs. Instrumentation such as piezometers, inclinometers, and seismic accelerometers would allow continuous validation of numerical predictions and the detection of early warning signs of instability.
- Methodological improvements: The hybrid pseudo-3D approach adopted here, while pragmatic, cannot fully capture the three-dimensional redistribution of stresses and deformations. Future research should therefore employ true 3D nonlinear finite element tools, coupled with stochastic ground motion simulations, to improve the accuracy of seismic response predictions.

- Field validation and regional applicability: Given the scarcity of empirical seismic dam performance data in Africa, future studies should emphasize field validation, including back-analysis of past seismic events and in-situ hydraulic monitoring. Extending the methodology to other embankment dams in the region would strengthen the generalizability of the conclusions.

In summary, the study confirms that coupled seismic-hydraulic analyses are indispensable for ensuring the resilience of large embankment dams. By explicitly considering rotational and torsional seismic effects, and by addressing seepage-stability interactions, the findings provide a foundation for updating design practices and safety assessment protocols for critical hydraulic infrastructure in Africa.

Appendix A

Table: Main characteristics of Memve'ele dam.

Parameter	Value
Dam type	Zoned embankment
Height	10.5 m
Crest length	622.5 m
Core material	Clay
Shell material	Rockfill
Reservoir capacity	82 million m^3

Geo-Studio Software

The internationally general software Geo-Studio 2007 is applied in this calculation, with the metric system of KN and m. Three modules of Geo-Studio including SEEP/W, SLOPE/W and SIGMA/W are used to complete the calculation. SEEP/W module can simulate any seepage problems that consider the flow is through saturated or unsaturated soils. SLOPE/W module can solve many slope stability problems by different methods such as Bishops Simplified, Janbu's Simplified, Morgenstern-Price and Spencer etc. SIGMA/W module is a finite element software product that can be used to perform stress and deformation analysis of earth structures. Its comprehensive formulation makes it possible to analyze both simple and highly complex problems.

SEEP/W module can simulate any seepage problems that consider the flow is through saturated or unsaturated soils. SLOPE/W module can solve many slope stability problems by different methods such as Bishop's Simplified, Janbu's Simplified, Morgenstern-Price and Spencer etc. SIGMA/W module is a finite element software product that can be used to perform

stress and deformation analyses of earth structures. Its comprehensive formulation makes it possible to analyze both simple and highly complex problems.

Appendix B

Factor of Safety

The factor of safety (FoS) quantifies the stability of a slope by comparing the forces resisting movement primarily shear strength, which comprises both frictional resistance and cohesion against those driving movement. It is defined as the ratio of resisting to driving forces:

$$\text{FoS} = \frac{\text{Resisting Forces (Shear Strength)}}{\text{Driving Forces}}$$

In the context of earth dam design, the minimum acceptable factor of safety typically does not exceed 1.5. While this may appear conservative, several justifications support this threshold:

Table 8: Results of earthquakes: Rotational forces acting on a circular and a composite slip surface

Material Strength Estimates: The values used for the strength of earth materials are generally conservative, selected near the lower bound of experimental measurements. In practice, the actual mobilized strength prior to failure is often substantially higher.

Time-Dependent Strength Gain: Over time, processes such as consolidation can lead to an increase in shear strength, implying that an initial factor of safety of 1.5 may increase to values near 2.0.

Conservative Loading Assumptions: Driving forces are usually estimated at their maximum plausible values, which may overstate actual field conditions.

According to the design practices of the U.S. Bureau of Reclamation (U.S.B.R.), a factor of safety of 1.5 is adopted under most conditions. However, recent designs for high dams have allowed for lower values down to 1.25 under conditions such as rapid reservoir draw-down or at the end of construction. For seismic loading, a factor of safety approaching unity is considered acceptable (Varshney et al., 1979).

Slope Protection

Slope protection is essential to safeguard the integrity of earth dams. The upstream slope must be shielded from wave action, while the downstream slope must be protected from

erosion due to rainfall. In some cases, additional measures are required to prevent damage from burrowing animals.

Common materials used for slope protection include:

Rock rip-rap; Concrete pavement; Steel facing; Bituminous pavement; Precast concrete blocks.

The U.S. Bureau of Reclamation recommends approximately 1 meter of dumped rock rip-rap over a 30-50 cm gravel filter layer, which has proven effective in major dam applications (Punmia and Pande, 1992).

Stability Formulations

1. Frictional Safety Factor Against Sliding

$$F_s = \frac{f\left(\sum P \sin\beta + \sum V \cos\beta - U\right) + cA}{\sum P \cos\beta - \sum V \sin\beta}$$

Where:

F_s: Sliding resistance factor of safety; f: Friction coefficient at the spillway sliding surface; ^{P}P: Sum of horizontal forces (kN); ^{P}V : Sum of vertical forces (kN); U: Uplift force (kN); c:

Cohesion (kPa); $A = L \times B$: Sliding surface area (m^2), with L: Length along the sliding surface (m); B: Width perpendicular to flow (m); β: Angle between the sliding surface and the horizontal.

2. Overturning Resistance Factor of Safety

$$K = \frac{\sum M_1}{\sum M_2}$$

Where:

K: Overturning resistance safety factor; $^{P}M_1$: Sum of anti-overturning moments (kNm);

$^{P}M_2$: Sum of overturning moments (kNm).

3. Foundation Base Pressure

$$\sigma_{\min}^{\max} = \frac{\left(\sum P \sin\beta + \sum V \cos\beta - U\right)}{A}\left(1 \pm \frac{6e}{L}\right)$$

Where: σ: Calculated base pressure (kPa), e: Eccentricity (m), given by:

$$e = \frac{L}{2} - \frac{\sum M}{\sum P \sin\beta + \sum V \cos\beta - U}$$

${}^{P}M = {}^{P}M_1 - {}^{P}M_2$: Net moment of the calculation section

4. Resultant Force Location (RFL)

The location of the resultant force on the foundation plane, useful for diagnosing overturning stability, is calculated as:

$$\text{RFL} = \frac{\sum M}{\sum P \sin\beta + \sum V \cos\beta - U}$$

This expression assists in determining whether the resultant lies within the middle third of the base, a condition favorable for structural stability.

Data availability

All data and models used in this study are available upon request from the corresponding author.

'Consent to Publish declaration: not applicable'.

'Consent to Participate declaration: not applicable'.

'Ethics declaration: not applicable.: not applicable'.

Author Contributions

Conceptualization, A; methodology, A, B and C; software, A, B and C; validation, A and B; formal analysis, A, B and C; investigation, A, B and C; resources, A, B and C; data curation, A, B and C; writing-original draft preparation, A, B and C; writing-review and editing, A.; visualization, A,B,C; supervision, A.; project administration, A.

Funding acquisition, nothing.

All authors have read and agreed to the published version of the manuscript.

Data availability: The data that support the findings of this study are available from the corresponding author, A, upon reasonable request.

Declarations:

Conflict of interest: The authors declare that they have no conflict of interest.

REFERENCES

[1] A. Kamanbedast and A. Delvari, Analysis of Earth Dam: Seepage and Stability Using Ansys and Geo-Studio Software, Iran, World Applied Sciences Journal 17 (9): 10871094, (2012).

[2] K. Abdelmalek, Analyse dynamique non linaire par lments finis des voiles en béton armé avec prise en compte des conditions du sol, Doctoral dissertation, Université de Batna 2-Mustafa Ben Boulaid, (2013).

[3] Basu D., Constantinou M. C., and Whittaker A. S., An equivalent accidental eccentricity to account for the effects of torsional ground motion on structures, Engineering Structures, 69:111, (2014).

[4] Basu D., Whittaker A. S., and Constantinou M. C., Characterizing rotational components of earthquake ground motion using a surface distribution method and response of sample structures, Engineering Structures, 99:685707, (2015).

[5] Bycroft G. N., Soil foundation interaction and differential ground motions, Earthquake Engineering and Structural Dynamics, 8:397404, (1980).

[6] Castellani A. and Boffi G., Rotational components of the surface ground motion during an earthquake, Earthquake Engineering and Structural Dynamics, 14:751767, (1986).

[7] De-La-Llera J. C. and Chopra A. K., Accidental torsion in buildings due to base rotational excitation, Earthquake Engineering and Structural Dynamics, 23:10031021, (1994).

[8] Elshemy M., Nasr R. I., Bahloul M. M., and Rashwan I. M., The effect of blockages through earth dams on the seepage characteristics, Faculty of Engineering, Tanta University, Egypt, (2002).

[9] P. Ndy Von Kluge, G. Djuidjé Kenmoé, and T. C. Kofané, Colliding solids interactions of earthquake-induced nonlinear structural pounding under stochastic excitation, Soil Dynamics and Earthquake Engineering, 132 (2020) 106065. https://doi.org/10.1016/j.soildyn.2020.106065.

[10] P. Ndy Von Kluge, G. Djuidjé Kenmoé, and T. C. Kofané, Application to nonlinear mechanical systems with dry friction: hard bifurcation in SD oscillator, SN Applied Sciences, 1 (2019), Issue 10:1140. DOI: 10.1007/s42452-019-0987-1.

[11] P. Ndy Von Kluge, G. G. Sengha, B. Doumia, G. Djuidjé Kenmoé, T. C. Kofané, Time-delayed state feedback control of stochastic resonance induced by rotational earthquake effects on non-smooth dynamic systems; International Journal of Dynamics and Control (2025) 13:337 https://doi.org/10.1007/s40435-025-01825-0

[12] P. Ndy Von Kluge, G. Djuidjé Kenmoé, and T. C. Kofané, Dry friction with various frictions laws: from wave modulated orbit to stick-slip modulated, Modern Mechanical Engineering, 5 (2015): 2840.

[13] P. Ndy Von Kluge, G. G. Sengha, W. Fokou Kenfack, L. L. Talla, G. Djuidje Kenmoé , and T. C. Kofané, Fractional dynamical behavior of a new nonlinear smooth and discontinuous (SD) oscillator for vibration energy harvesting with nonlinear magnetic coupling, Eur. Phys. J. Plus (2023) 138:937. https://doi.org/10.1140/epjp/s13360-023-04559-0.

[14] Paul Ndy Von Kluge, Nonlinear Pounding and Engineering Failure Analysis of Non-smooth Structural Systems Subjected to Stochastic Excitations, PhD Thesis, University of Yaoundé I, (Defense 29 April 2021).

[15] Hasani H., Mamizadeh J., and Karimi H., Stability of Slope and Seepage Analysis in Earth Fills Dams Using Numerical Models (Case Study: Ilam Dam), Iran, World Applied Sciences Journal, 21 (9): 13981402, (2013).

[16] Hart G., DiJulio M., and Lew M., Torsional response of high-rise buildings, Journal of Structural Division, ASCE, 101:397414, (1975).

[17] Ismail M. A. M., Ng S. Min, and Gey K., Stability Analysis of Kelau Earth-Fill Dam Design under Main Critical Conditions, Malaysia, Electronic Journal of Geotechnical Engineering (EJGE), (2012).

[18] Kirra M. S., Shahien M., Elshemy M., and Zeidan B. A., Seepage and Slope Stability Analysis of Mandali Earth Dam, Iraq: A Case Study, International Conference on Advances in Structural and Geotechnical Engineering, ICASGE15, 69 April 2015, Hurghada, Egypt.

[19] Kratochvil J., Numerical modeling of Non-stationary Free Surface Flow in Embankment Dams, Brno University of Technology, Czech Republic, (2004).

[20] Lambe T. W. and Whitman R. V., Soil Mechanics, John Wiley and Sons, Inc., SI Version, New York, USA, (1979).

[21] Nippon Koei Co. Ltd., The Early Feasibility Report, (1993).

[22] Newmark N. M., Torsion in symmetrical buildings, Proceedings of the Fourth World Conference on Earthquake Engineering, Santiago, Chile, pp. 1932, (1969).

[23] Politopoulos I., Response of seismically isolated structures to rocking-type excitations, Earthquake Engineering and Structural Dynamics, 39:325342, (2010).

[24] Bessoles B. and Trompette R., La chaine panafricaine zone mobile dAfrique Centrale (Partie Sud) et zone mobile soudanaise, Mmoires du B.R.G.M., 92, 401 p., (1980).

[25] Stability Modeling with SLOPE/W 2007, GEO-SLOPE International, Ltd, Canada.

[26] Stress-Deformation Modeling with SIGMA/W 2007, GEO-SLOPE International, Ltd, Canada.

[27] Seepage Modeling with SEEP/W 2007, GEO-SLOPE International, Ltd, Canada.

[28] Sheikhabadi M. R. F., Simplified relations for the application of rotational components to seismic design codes, Engineering Structures, 59:141152, (2014).

[29] Tatewar S. P. and Pawade L. N., Stability Analysis of Earth Dam by Geostudio Software, India, International Journal of Civil Engineering and Technology (IJCIET), Volume 3, Issue 2, JulyDecember (2012).

[30] ULDC, Urban Levee Design Criteria, Engineering Criteria and Guidance for the Design, California Department of Water Resources, May (2012).

[31] Wolf J. P., Obernhueber P., and Weber B., Response of a nuclear plant on aseismic bearings to horizontally propagating waves, Earthquake Engineering and Structural Dynamics, 11:483497, (1983).

[32] Zienkiewicz O. C. and Taylor R. L., The Finite Element Method, Vols. I & II, 5th Edition, McGraw-Hill, (1967).

[33] Zembaty Z. and Boffi G., Effect of rotational seismic ground motion on dynamic response of slender towers, European Earthquake Engineering, 8:311, (1994).

[34] Zomorodian S. M. and Abodollahzadeh S. M., Effect of Horizontal Drains on Upstream Slope Stability During Rapid Drawdown Condition, Shiraz University, Iran, International Journal of Geology, Issue 4, Volume 4, (2010).

[35] Techniques on the seismic performance of RC buildings, Discover Civil Engineering, 2, 94 (2025). https://doi.org/10.1007/s44290-025-00253-5.

Citation: Gérard Ghislain SENGHA, Paul NDY VON KLUGE, Bénoît DOUMIA. (2026). Integrated Seismic-Hydraulic Performance Assessment of a Zoned Embankment Dam: Application to the Memve'ele Hydropower Project (Cameroon). International Journal of Civil Engineering and Technology (IJCIET), 17(2), 13-57.

Abstract Link: https://iaeme.com/Home/article_id/IJCIET_17_02_002

Article Link:
https://iaeme.com/MasterAdmin/Journal_uploads/IJCIET/VOLUME_17_ISSUE_2/IJCIET_17_02_002.pdf

✉ **editor@iaeme.com**